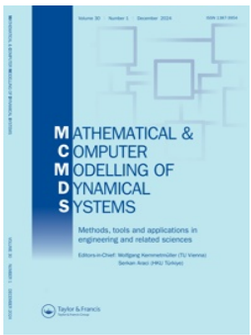

Taylor & Francis
Taylor & Francis Group

Mathematical and Computer Modelling of Dynamical Systems

Methods, Tools and Applications in Engineering and Related Sciences

ISSN: (Print) (Online) Journal homepage: www.tandfonline.com/journals/nmcm20

Computational approaches on integrating vaccination and treatment strategies in the SIR model using Galerkin time discretization scheme

Attaullah, Khaled Mahdi, Mehmet Yavuz, Salah Boulaaras, Mohamed Haiour & Viet-Thanh Pham

To cite this article: Attaullah, Khaled Mahdi, Mehmet Yavuz, Salah Boulaaras, Mohamed Haiour & Viet-Thanh Pham (2024) Computational approaches on integrating vaccination and treatment strategies in the SIR model using Galerkin time discretization scheme, Mathematical and Computer Modelling of Dynamical Systems, 30:1, 758-791, DOI: 10.1080/13873954.2024.2405504

To link to this article: https://doi.org/10.1080/13873954.2024.2405504

Published online: 16 Oct 2024.

MATHEMATICAL AND COMPUTER MODELLING OF DYNAMICAL SYSTEMS
2024, VOL. 30, NO. 1, 758–791
https://doi.org/10.1080/13873954.2024.2405504

Taylor & Francis
Taylor & Francis Group

Computational approaches on integrating vaccination and treatment strategies in the SIR model using Galerkin time discretization scheme

Attaullah[a], Khaled Mahdi[b,c], Mehmet Yavuz[d], Salah Boulaaras[e], Mohamed Haiour[f] and Viet-Thanh Pham[g]

[a]Department of Mathematics & Statistics, University of Chitral, Chitral, KP, Pakistan; [b]Department of Physics, Faculty of Sciences, M'Sila University, M'Sila, Algeria; [c]Physics Energy Laboratory, Constantine 1 University, Constantine, Algeria; [d]Department of Mathematics and Computer Sciences, Necmettin Erbakan University, Konya, Türkiye; [e]Department of Mathematics, College of Science, Qassim University, Buraydah, Saudi Arabia; [f]Numerical Analysis, Optimization and Statistics Laboratory, University Badji Mokhtar, Annaba, Algeria; [g]Faculty of Electronics Technology, Industrial University of Ho Chi Minh City, Ho Chi Minh City, Vietnam

ABSTRACT

In this manuscript, we carried out a thorough analysis of the general SIR model for epidemics. We broadened the model to include vaccination, treatment, and incidence rate. The vaccination rate is a testament to the alternatives made by individuals when it comes to receiving vaccinations and merging with the community of the recovered. The treatment rate measures how often people who have contracted a disease are able to transition into the recovered category. The continuous Galerkin-Petrov method, specifically the cGP(2)-method, is employed to calculate the numerical solutions of the models. The cGP(2)-method imperative to analyse two unknowns over every time interval. The unknowns can be determined by solving a block system of size (2×2). This approach demonstrates a strong level of precision throughout the entire time interval, with an impressive rate of convergence at the discrete time points. In addition, the article investigates the concept of the basic reproduction number (R_0) and explores the intricacies of conducting sensitivity analysis of the developed system.

ARTICLE HISTORY
Received 7 June 2024
Accepted 12 September 2024

KEYWORDS
SIR model; vaccination and treatment control; numerical method; numerical method; dynamical behavior; numerical methods

1. Introduction

It is frequently identified that when there is an upsurge in the number of casualties caused by infectious diseases in humans, they actively search for remedies. They are dedicated to understanding the origins of infections and taking the appropriate medical measures. When a new infectious disease emerges, the options for treatment are often scarce and come with an exorbitant cost. Consequently, people are constantly searching for efficient and reliable control techniques that can be immediately put through behaviour.

CONTACT Salah Boulaaras s.boularas@qu.edu.sa Department of Mathematics, College of Science, Qassim University, Buraydah 51452, Saudi Arabia

Specifically, it demonstrates a strong curiosity in areas where the standard of living is below average. Several experiments have been conducted for the treatment, such as vaccinations, antibiotics, and increasing awareness. The improvements that were made in sanitation, antibiotics, and vaccination policies culminated in a notable enhancement in public health during the latter half of the previous century. This advancement led to the possibility of eliminating viral diseases. Due to this rationale, diseases like cancer and cardiovascular conditions are given more prominence. Nevertheless, viral diseases have evolved into different manifestations, leading to the emergence of novel illnesses and the alteration of current epidemics. Other approaches, aside from these, are of great importance when it comes to taking precautions. In developed countries, there has been an evolution from non-communicable diseases (NCDs) to communicable viral diseases (CVDs) (Parkin et al. 1999; WHO 2003). In tropical and subtropical regions, The human immunodeficiency virus (HIV) is a major epidemic that poses significant challenges in terms of economics, health, and social impact (See Aron and Robert 1982; Attaullah Sohaib and Sohaib 2020; Attaullah Jan et al. 2021; Attaullah Alyobi et al. 2022; Attaullah et al. 2022, 2023) for detail information). Jan et al. (2023) explored the optimization of the fractional-order parameter and conducted an error analysis for human immunodeficiency virus under the Caputo operator. Dhahbi et al. (2022) discussed the spread of the coronavirus disease 2019 (COVID-19) pandemic in Saudi Arabia by utilizing a simplified discrete version of the Gompertz model. Attaullah et al. (2023) have created an innovative mathematical model of COVID-19 and successfully solved it using a higher order Galerkin time discretization scheme. These types of diseases transmitted by vectors pose significant risks to regions around the Mediterranean. Elbasha and Galvani (2005) investigated the development of vaccination strategies to tackle various types of Human infection virus. Prevention is crucial in the fight against AIDS, as there is currently no vaccine available for its complete elimination. The Dengue virus has affected warm regions across the globe, such as India, Sri Lanka, Central Asia, China, Central America, and Pakistan. The occurrence of AIDS in urban areas varies from that in rural areas. It has been observed that dengue has become widespread in more than a hundred countries worldwide in the last years. The unfavourable environmental conditions and inadequate sanitation contribute to the spread of disease (Rodrigues et al. 2013). Mathematical models provide a strong framework for studying infections. Anderson et al. (1992) conducted a study on infectious diseases using mathematical models. The early vector-borne diseases reviewed by Rogers et al. (1988). Jan et al. (2023) presented a fractional model that explains the dynamics of transmission in dengue infection when vaccination is involved. Sabir et al. (2022) conducted a numerical study on a fractional nonlinear dengue model, employing artificial neural networks. The further research on Dengue Fever (DF) explored (Esteva and Vargas 1998). Derouich et al. (2003) gave his views when he studied the dynamic of DF caused by two different type of vectors. Dengue caused by four different serotypes distinguished as DEN1, DEN2, DEN3, DEN4 (Classification, Medical Microbiology 1996; Ryan et al. 2004; Tomashek 2011). It is noted that a person caught once by one of the serotype cannot be infected again by the same serotype. This is due to homologous immunity but due to loose immunity known as heterologous immunity the individual becoming more susceptible for other three sero types. This should lead to the DHF. The second type of infection is more dangerous and may lead towards death. Consequently, mathematical modelling became an interesting

and beneficial way for the control of such epidemic diseases. Better strategies can propose for understanding illness by using mathematical models. Favier et al. (2005) discovered the effects of multi-breed entity on advent of some disease. Focks et al. (1995) proposed the stochastic models to stimulate the infection. Degallier et al. (2009); Kongnuy et al. (2011) checked the time evolution of dengue infection with the application of statistical methods by collecting data from Brazil and Thailand. Primary prevention depends upon the two states of vectors adult mosquito and larva control according to the intended target (Natal 2002). Mathematical modelling for the treatment of vector-borne ailment plays a vital role and gave proper way of cure. In parallel to mathematical models simpler approaches like local screening, air-filtring and other ways are effective to resist dengue (Dat and Lesser 2013). Vector borne diseases range from childhood disease small pox to diseases that cause death, such as acquired immune deficiency syndrome. The research of Feng and Hernandez (1997) investigated into the intricate dynamics of vector–host interactions within a two-strain epidemiological system. They focused on determining the basic reproduction number of the model in a population where all hosts are susceptible. Kermack and Anderson (1932) introduced the Susceptible Infected Removed (SIR) model for a fixed population, which encompasses individuals who are susceptible, infected, and recovered. The host population is organized into compartments, where each compartment is made up of individuals who have the same disease. Throughout history, a range of numerical techniques have been utilized to solve epidemic models. Laarabi et al. (2014) conducted a study on the SIRS model, exploring the effects of vaccination and treatment control. Dengue has been investigated by using numerous mathematical models, and a number of models are source of population explicitly (Esteva and Vargas 2000; Wearing and Rohani 2006; Medlock et al. 2009). Alongside explicit formulation, some of the models present mosquito population in implicit form in the transmission term (Cummings et al. 2005; Adams et al. 2006; Nagao and Koelle 2008). Khalid et al. (2015) studied the susceptible, infected, recovered model of Dengue by using the technique of Perturbation Iteration Algorithm (PIA). By using this method it has been shown that solution can be determined in the form of convergent series. Yusuf and Benyah (2012) proposed SIR model by considering variable population and further developed a problem with vaccination and treatment strategies as a tool of control. The analysis of this model ensures that epidemic free balance point is universally asymptotically stable until the value of the threshold parameter remains below unity. Optimal level of both control strategies presented by using Pontryagin's maximum principle (PMP). The transmission model of dengue with constant human population discussed by Kongnuy and Pongsumpun (2011). The disease-free equilibrium state determined by a threshold parameter known as the basic reproduction number. Fathalla and Rihan (2012) investigated the delayed SIR model qualitatively and found the conditions to ensure the stability of the corresponding steady state. Altaf et al. (2015) proposed the epidemic model by including non-linear saturated incidence rate and discussed the stability of both endemic and disease free equilibrium points. They also found the threshhold parameter for analysis of stability. Naz et al. (2015) analysed exact as well as integral solutions of epidemiology models using partial Lagrangian approach. They replaced three first order nonlinear differential equations into a system of one first order and a second order equation. The complex dynamics induced by antibody-dependent enhancement taking human population as variable whereas vector population constant explored by

Wan and Cui (2009). They also calculated basic reproduction for stability endemic equilibrium point. Kongnuy et al. (2011) investigated the transmission of dengue in pregnancy and infancy by using mathematical models simulations. Samat and Percy conducted a study on numerical solutions of the SIR model for epidemic transmission, which is described by a non-linear ordinary differential equation. A technique is presented for solving the SIR model, which involves converting the continuous time scale into a discrete time scale that is densely populated. The data was collected from Kuala Lumpur Malaysia. Dietz et al. (1993) explored that basic reproduction commonly used to calculate the worth of epidemic. Wang et al. (2024) applied the SIR model to analyse the transmission of influenza A in Ningbo, covering the period from 1 January 2023 to 30 June 2023. The available data only includes the daily newly confirmed cases, while information about the daily number of infected individuals and recovered individuals remains undisclosed. The exact number of individuals who are susceptible to exposure risk remains uncertain. Due to the limited data available, the parameter estimation problem of the SIR model is converted into an optimization problem. The Particle Swarm Optimization algorithm is employed to tackle the optimization problem. The model accurately captures the patterns and dynamics of the widespread transmission of influenza A, aligning closely with real-world observations in the post-COVID-19 era. Kalachev et al. (2024) developed a simple modification to the SIR model to estimate the percentage or ratio of reported infection cases. The proposed modification entails adjusting the classical SIR model to produce a mathematically equivalent version that explicitly incorporates the reporting parameter. They showcased the validation of the proposed method by employing simulated data with known disease cases. Subsequently, they applied the method to two real-world data sets to estimate the proportion of reported cases in Missoula County, Montana, U.S.A. The data sets used were the flu data for 2016–2017 and the COVID-19 data for the autumn of 2020. Olu et al. (2024) analysed the dynamics of the SIR model in the context of the COVID-19 outbreak in Nigeria during the year 2020. The model is validated by fitting it to data on the prevalence and active cases of COVID-19, sourced from a government agency responsible for disease control. They utilized the Sumudu Decomposition Method (SDM) to numerically solve the model and then compared its results with the commonly used Runge-Kutta fourth-order method. Kumar and Abbas (2022) initiated a detailed conversation about an age-structured SIR model, exploring how the transmission of disease occurs not only through direct person-to-person interactions but also through indirect contacts. The model was formulated as an abstract semi-linear Cauchy problem in a suitable Banach space to demonstrate the existence of a solution. Additionally, the existence of steady states was also established. They also numerically solved the model to analyze the impact of indirect contacts on the density of infected individuals. Centres et al. (2024) conducted a study on the spread of an epidemic using a model of agent diffusion. They applied the SIR model and examined two potential contagion mechanisms. The first mechanism involved a susceptible agent becoming infected if it came into contact with an infected agent, with a certain probability. The second mechanism involved a group of susceptible agents within a specific radius of an infected agent, where each susceptible agent had a probability of becoming infected. Ma et al. (2024) carrying out a thorough analysis of the stability of the SIRS model, implementing the effects of pulse vaccination and elimination disturbance. The findings indicate that in order to halt the spread of the disease, it is crucial to carefully select the optimal vaccination rate, elimination rate, and

impulsive period. Marca et al. (Ma et al. 2024) derived the SIR model by analyzing a multi-agent system, where individuals are categorized based on their epidemiological compartment and viral load. They applied the microscopic dynamics to the appropriate kinetic equations, which ultimately lead to the derivation of the macroscopic equations for the densities and viral load momentum of the compartments. They thoroughly examined the scenario where the transmission rate is linked to the viral load and compared it to the traditional case with a constant transmission rate. Romanullah and Islam (2013) proposed the general SIR model and discuss the stability. They also found the basic reproduction number and found the numerical solution by using RK-4 method. Hu et al. (2012) proposed SIR model with non linear incidence and treatment rate. Zaman et al. (2008) proposed SIR model with vaccination control and determined the stability. We studied SIR model of epidemics in general form and found the solution by using cGP(2)-method (Schieweck 2010; Hussain 2011; Hussain et al. 2011). The model is extended by using vaccination, treatment and incidence rates. The vaccination and treatment rate are very effective on susceptible and infected individuals population. These rates effects significantly susceptible and infected individuals converge to recovered population. Both of the models solved by using RK-4 method and cGP(2) methods.

2. Mathematical model of epidemic

This section explores the general SIR model for epidemics proposed by Romanullah and Islam (2013). In the model, the entire population is divided into three compartments: susceptible individuals S(t), infected individuals I(t), and recovered individuals. The model consists of a complex system of ordinary differential equations that categorized the population into three distinct compartments. Here is the SIR model:

$$\begin{aligned} \tfrac{dS}{dt} &= \mu - \lambda S(t)I(t) - \mu S(t), \\ \tfrac{dI}{dt} &= \lambda S(t)I(t) - \gamma_1 I(t) - \mu I(t), \\ \tfrac{dR}{dt} &= \gamma_1 I(t) - \mu R(t). \end{aligned} \tag{1}$$

The initial conditions and detailed information of all the parameters used in the model are visualized in Table 1.

2.1. *Basic reproduction number* (R_0)

In this section, we find the basic reproduction number, for this we will put the right hand side of equation (1) equals to zero. Also, put $S = S_0$ and $I = I_0$ and this leads to:

$$\mu - \lambda S_0(t)I_0(t) - \mu S_0(t) = 0, \tag{2}$$

$$\lambda S_0(t)I_0(t) - \gamma_1 I_0(t) - \mu I_0(t) = 0. \tag{3}$$

Equation (2) yields

Table 1. The detail explanation and values of the parameters used in the model.

Variables	Description	Values	Ref.
$S(0)$	Susceptible (individuals who can contract the disease)	120 peoples	(Romanullah and Islam 2013)
$I(0)$	Infected (individuals capable of transmitting the disease to others)	80 peoples	(Romanullah and Islam 2013)
$R(0)$	Recovered (individuals who have acquired immunity)	40 peoples	(Romanullah and Islam 2013)
μ	Natural death rate of population	$0.1\,UT^{-1}$	
λ	Effective contact rate between susceptible and infected individuals	$0.0098\,people^{-1}$	(Romanullah and Islam 2013)
γ_1	The recovery rate of infected individuals	$0.5\,people^{-1}$	(Romanullah and Islam 2013)
β	Transmission rate	$0.0001 people^{-1}UT^{-1}$	(Romanullah and Islam 2013)
α	Mortality rate caused by illness	$0.01UT^{-1}$	(Kongnuy et al. 2011)
u_1	Effectiveness of vaccination	$0-1$	(Kongnuy et al. 2011, Natal 2002)
u_2	Effectiveness of treatment	$0-1$	(Kongnuy et al. 2011, Natal 2002)

$$S_0(t) = \frac{\mu}{\lambda I_0(t) + \mu}. \tag{4}$$

If we put $I_0 = 0$ in Equation (2) then we will get the disease free equilibrium point $E(1, 0)$.

For endemic equilibrium point $E(S_e, I_e)$, put $S = S_e(t)$ and $I = I_e(t)$ in equation (3). We obtain,

$$\begin{aligned}
&\mu - \lambda S_e(t) I_e(t) - \mu S_e(t) = 0,\\
&\lambda S_e(t) I_e(t) - \gamma_1 I_e(t) - \mu I_e(t) = 0,\\
&(\lambda S_e(t) - \gamma_1 - \mu) I_e(t) = 0,\\
&(\lambda S_e(t) - \gamma_1 - \mu) = 0,\\
&S_e(t) = \tfrac{\gamma_1+\mu}{\lambda}.
\end{aligned} \tag{5}$$

By putting value of $S_e(t)$ from Equation (5) into Equation (2), we obtained

$$\begin{aligned}
&\mu - \lambda \tfrac{\gamma_1+\mu}{\lambda} I_e(t) - \mu \tfrac{\gamma_1+\mu}{\lambda} = 0,\\
&\mu - (\mu + \gamma_1) I_e(t) - \tfrac{\mu(\mu+\gamma_1)}{\lambda} = 0,\\
&(\mu + \gamma_1) I_e(t) = \mu - \tfrac{\mu(\mu+\gamma_1)}{\lambda},\\
&I_e(t) = \tfrac{\mu}{(\mu+\gamma_1)} - \tfrac{\mu(\mu+\gamma_1)}{\lambda(\mu+\gamma_1)},\\
&I_e(t) = \tfrac{\mu}{\mu+\gamma_1} - \tfrac{\mu}{\lambda},\\
&I_e(t) = \tfrac{\mu}{\lambda}[\tfrac{\lambda}{\mu+\gamma_1} - 1],\\
&I_e(t) = \tfrac{\mu}{\lambda}[R_0 - 1].
\end{aligned} \tag{6}$$

The value of $R_0 = \frac{\lambda}{\mu+\gamma_1}$ is often recognized as the basic reproduction number. The basic reproduction number is of great importance in mathematical epidemiology, as it plays a critical role as a threshold parameter. The basic reproduction number is a measure that quantifies the average number of offspring produced by an individual in a population of susceptible individuals. The spread of an infectious disease among a population is a vital aspect of these types of illnesses. This can be accomplished by delving into the core concept

of the reproduction number. If the value of R_0 is less than 1, then the average number of infected individuals produced by each infected individual over the entire period of infection will be less than one. When the disease free equilibrium is achieved, it signifies that the system is locally asymptotically stable, suggesting that the disease has been completely eliminated from the population. If the value of R_0 exceeds 1, then each infected individual will produce multiple infections when interacting with susceptible individuals during the entire period of infectivity. This leads to the spread of illness among the population. Now, by applying Lyapunov function theory, we can conclude that the epidemic model proposed in is globally asymptotically stable.

Theorem 1. If the value of R_0 is less than or equal to 1, the disease free equilibrium E_0 of the system is globally asymptotically stable on the given domain Ω.

Proof: In order to confirm the global stability of the disease-free equilibrium, we establish the Lyapunov function.

$$V : \Omega \rightarrow R:$$

$$V(S, I) = I(t)$$

Deriving the time derivative of V along the proposed system solution (Romanullah and Islam 2013).

$$\frac{dV}{dt} = \frac{dI}{dt}. \tag{7}$$

Putting the value of $\frac{dI}{dt}$ from Equation (1) in

$$\begin{aligned} \tfrac{dV}{dt} &= \lambda S(t)I(t) - \gamma_1 I(t) - \mu I(t), \\ \tfrac{dV}{dt} &= (\gamma_1 + \mu)\left[\tfrac{\lambda}{\gamma_1+\mu} S(t) - 1\right] I(t), \\ \tfrac{dV}{dt} &= (\gamma_1 + \mu)[R_0 S(t) - 1] I(t). \end{aligned} \tag{8}$$

From Equation (8) it is clear that
$\frac{dV}{dt}$ is non-positive that is $\frac{dV}{dt} \leq 0$ for $R_0 < 1$.
If $R_0 < 1$ then $\frac{dV}{dt} = 0$ if and only if $I(t) = 0$.
Suppose $I(t) = 0$ then by plugging value in we obtained $\frac{dV}{dt} = 0$
Conversely,
Suppose $\frac{dV}{dt} = 0 \Rightarrow (\gamma_1 + \mu)[R_0 S(t) - 1] I(t) = 0$,$(\gamma_1 + \mu) \neq 0$, since $\gamma 1 \neq 0$ and $\mu \neq 0$
$[R_0 S(t) - 1] \neq 0$ since $R_0 S(t) \neq 1$
Hence $I(t) = 0$.
If $R_0 = 1$, then $\frac{dV}{dt} = 0$ if and only if $S(t) = 1$. We will prove this necessary and sufficient condition.
Suppose $R_0 = 1$ and $S(t) = 1$ We have to prove $\frac{dV}{dt} = 0$.
In view of our supposition right hand side of equation of $\frac{dV}{dt} = 0$ yields $\frac{dV}{dt} = 0$.
Conversely,

Suppose $\frac{dV}{dt} = 0$ and $R_0 = 1$. We have to prove $S(t) = 1$. Putting $\frac{dV}{dt} = 0$ and $R_0 = 1$ in last equation of we obtain $(\gamma_1 + \mu)[S(t) - 1]I(t) = 0$, $(\gamma_1 + \mu) \neq 0$. Therefore, $I(t) = 0$ or $S(t) - 1 = 0$.

Hence $S(t) - 1 = 0 \Rightarrow S(t) = 1$ and this complete the proof.

In view of LaSalle's invariant principle (Romanullah and Islam 2013) the disease free point E_0 is globally asymptotically stable on Ω. □

3. Time discretization of SIR model using cGP(2)-method

In this section, we provide a comprehensive overview of the time discretization scheme. We delve into the mathematical foundations of the cGP(2)-method and demonstrate its implementation for solving the SIR model proposed by Romanullah and Islam (2013). The system of ordinary differential equations for the SIR model can be illustrated as follows: Consider the time interval $I = [0, \top]$ with the final time $\top$ that is greater than zero. We identified a function $v : I \rightarrow W$ such that

$$\begin{aligned} \mathbf{v}(t) &= (S(t), I(t), R(t)), \\ \mathbf{v}(0) &= (S(0), I(0), R(0)), \\ \mathbf{v}'(t) &= G(t, v(t)) \quad t \in (0, \top), \\ \mathbf{v}(0) &= v_0, \end{aligned} \tag{9}$$

where the derivative of $\mathbf{v}(t)$ with respect to time is denoted as $\mathbf{v}'(t)$ and the initial value at time $t = 0$ is represented by $\mathbf{v}_0 \in \mathbf{W}$. The vector $\mathbf{v}(t)$ belongs to the set $\mathbf{W}$, where $\mathbf{W}$ is defined as R^{α_I}. It represents the nodes of the semi-discrete finite element solution $v_I(t)$ for a parabolic differential equation:

$$\mathbf{v}_I(t) = \sum_{j=1}^{\alpha_I} \mathbf{v}_j(t) c_j \text{ and } \mathbf{W}_I = \text{span}\{c_j : j = 1, \ldots, \alpha_I\}. \tag{10}$$

The function $G : I \times \mathbf{W} \rightarrow \mathbf{W}$ is almost nonlinear and can be regarded as appropriately smooth. Here, we provide the notations utilized for the time discretization of problem (2). To analyze the smoothness of the function $t \rightarrow \mathbf{v}(t)$, we will carefully examine a subinterval of $J \subset I$. We are exploring a space known as $C^n(J, \mathbf{W})$, which encompasses functions on J that possess n levels of continuous differentiability and have values in W. This space is defined by the utilization of semi-norm and norm.

$$\begin{aligned} ||v||_{c^n(J,W)} &= \max sup ||v^{(k)}(t)||_W, \\ |v|_{c^n(J,W)} &= \sup ||v^{(n)}(t)||_W. \end{aligned} \tag{11}$$

Consider establishing the subintervals by dividing I into N subintervals, denoted as $I_n = (t_{n-1}, t_n)$. This will result in a set of subintervals known as the time-mesh. The value of R_τ,where τ represents the time discretization parameter, which is chosen as the maximum value. It is defined as follows: $\tau = \max_{1 \leq n \leq N\tau_n}$ and $\tau_n = t_n - t_{n-1}$. Let R_τ be the set consisting of $I_1, I_2, I_3 \cdots I_N$ represents the interval (t_{n-1}, t_n). For $n = 1, 2, 3, \cdots, N$ and $0 = t_0 < t_1 < \cdots < t_N = T$. We will utilize the space $L^2(I, \mathbf{W})$ which is defined as follows: $L^2(I, W)$ consists of functions v that map from I to $\mathbf{W}$ and satisfy the condition $||v||_{L^2_{(I,W)}}$. The set of all functions v in $L^2(I, W)$ such that the L^2 norm of v is finite, where

the L^2 norm of v is defined as the square root of the integral of the squared norm of v over I. In order to approximate the solution $\mathbf{v} : I \to \mathbf{W}$. In our approach, we consider a piecewise polynomial $\mathbf{v}_\tau : I \to \mathbf{W}$ transform into $\mathbf{W}$ within a time t of magnitude k, meaning that we are searching for v_τ in either continuous time-discrete space

$$\mathbb{M}_k^c(R_\tau) = \{\mathbf{v} \in C(I, \mathbf{W}) : \mathbf{v}|_{I_n} \in \mathbb{M}_k(I_n, \mathbf{W}), \quad I_n \in R_\tau\}, \tag{12}$$

or in discontinuous time discrete space

$$\mathbb{M}_k^{\alpha c}(R_\tau) = \{\mathbf{v} \in L^2(I, \mathbf{W}) : \mathbf{v}|_{I_n} \in \mathbb{M}_k(I_n, \mathbf{W}), \quad I_n \in R_\tau\}. \tag{13}$$

For discrete function $\mathbf{v} : I \to \mathbf{W}$, which are not continuous at the right and left end points of time subintervals, we define the right and left sided values $\mathbf{v}_n^+$ and $\mathbf{v}_n^-$ and the jumps $[\mathbf{v}_\tau]_n$ respectively as:

$\mathbf{v}_n^+ = \lim_{t \to t_{n+}} \mathbf{v}_\tau(t)$, $\mathbf{v}_n^- = \lim_{t \to t_{n-}} \mathbf{v}_\tau(t)$, $[v]_n = \mathbf{v}_n^- - \mathbf{v}_n^+$.

We also define the function values on $\mathbf{v}_\tau(t)$ with $n \geq 1$ the interval $I_n = (t_n, t_{n-1})$ will be $\mathbf{v}_\tau(t_n) = \mathbf{v}_n^-$, $\mathbf{v}_\tau(0) = \mathbf{v}_0$.

At this point, we use $\mathbb{M}_{k-1}^c(R_\tau)$ as our discrete test space, while the space $\mathbb{M}_k^c(\mathrm{R}_\tau)$ is used as the solution space for time discretization. Given the initial conditions in Equation (4), the discrete solution $\mathbf{v}_\tau$ has a considerable number of degrees of freedom, referred to as N.k. The test space has a dimension of $N.k$. To determine the unknown coefficients of $\mathbf{v}_\tau$, we need to initially transform Equation (9) into integral form, commonly known as variational or weak form. In order to address this issue, we can multiply the provided equation by a suitable test function and integrate it over the domain I. This process will lead to a specific issue referred to as a time-discrete global problem. It is essential that a test function satisfies the necessary requirements of having a valid integral.

Find $\mathbf{v}_\tau \in_k^c (R(_\tau)$ such that $\mathbf{v}_\tau(0) = \mathbf{v}_o$ and

$$\int_I < \mathbf{v}^{'}(t), v_\tau(t) > dt = \int_I < \mathbf{G}(t, \mathbf{v}_\tau(t)), v_\tau(t) > dt, \quad v_\tau \in \mathbb{M}_{k-1}^{\alpha c}(R_\tau), \tag{14}$$

where $< ., . >$ denotes the standard inner product in $\mathbf{W} = R^\alpha$. This specific discretization is known as the exact continuous Galerkin-Petrov method of order k, or just the exact cGP(k)-method. The Galerkin-Petrov name was determined because the test space $\mathbb{M}_{k-1}^{\alpha c}(R_\tau)$ is different from the ansatz space $\mathbb{M}_k^c(R_\tau)$. Be sure to carefully determine the time integral on the right side of Equation (14). Given that the discrete test space $\mathbb{M}_{k-1}^{\alpha c}(R_\tau)$ is not continuous, a possible approach to solving problem (14) is by employing a time-marching process. This involves solving local problems on the time intervals sequentially. In order to accomplish this goal, we decide a test function $v_\tau(t) = v\Omega(t)$, where v is a constant from the set of real numbers and Ω is a scalar function defined on the interval I. The function Ω is zero on the subinterval $I|I_n$ and a polynomial of degree less than or equal to $k-1$ on the subinterval I_n. Then, we can derive the problem of exact cGP(k)-method from Equation (1), which is referred to as:

$$\int_{I_n} < \mathbf{v}^{'}(t), v > \Omega(t) dt = \int_{I_n} < G(t, \mathbf{v}_\tau(t)), v > \Omega(t) dt, \quad v \in \mathbf{W}, \quad \Omega \in M_{k-1}(I_n). \tag{15}$$

For any given value $n \geq 2$, $\mathbf{v}_{n-1}^- = \mathbf{v}_\tau|I_{n-1}(t_{n-1})$ and for $n = 1$, $\mathbf{v}_{n-1}^- = \mathbf{v}_0$.

In order to solve the integral on the right hand side of equation (15) numerically, we need to consider non-linear functions. If the integrated function is a polynomial with a degree of less than or equal to $(2k-1)$, then the $(k+1)$-point Gauss-Lobatto formula is exact. This represents why we use this formula on the left-hand side of equation (15) to calculate the exact value. Now, we will examine the reference interval $\hat{I}=[-1,1]$. Consider the values of $\hat{I}=[-1,1]$. Let $t_{j,j}=0,\ldots,k$, and let $\hat{\mu}$ represent the nodes and weights on $\hat{I}$. This leads to the I_n-problem of numerically integrated cGP(k)-methods, where we must determine $\mathbf{v}_\tau|_{I_n}\in\mathbb{M}_k(I_n,\mathbf{W})$, such that

$$\begin{aligned}&\sum_{j=0}^{k}\hat{\rho}_j\mathbf{v}_\tau'(t_{n,j})\Omega(t_{n,j})=\sum_{j=0}^{k}\hat{\rho}G(t_{n,j},\mathbf{v}_\tau(t_{n,j}))\Omega(t_{n,j}),\\&\mathbf{v}_\tau(t_{n-1})=v_{n-1}\quad\Omega\in\mathbb{M}_{k-1}(I_n).\end{aligned}\tag{16}$$

We obtain $\mathbf{v}_\tau|_{I_n}$ by using the polynomial ansatz which is

$$\mathbf{v}_\tau(t)=\sum_{j=0}^{k}\mathbf{V}_n^j\boldsymbol{\phi}_{n,j}(t)\quad t\in I_n.\tag{17}$$

The functions $\boldsymbol{\phi}_{n,j}$ represent the Langrange basis functions with $k+1$ nodal points $t_{n,j}\in\tilde{I}_n$. The functions $\boldsymbol{\phi}_{n,j}$ fulfil the specified conditions:

$$\boldsymbol{\phi}_{n,j}(t_{n,j})=\delta_{i,j}\text{ where }i,j=0,1,\cdots,k,\tag{18}$$

In the present instance, the symbol $\delta_{i,j}$ is used to represent the Kronecker symbol, which is known for satisfying certain axioms. One of these axioms states that $\delta_{i,j}$ is equal to 1. When i is equal to j, and $\delta_{i,j}$ is equal to zero,For $i\neq j$

We select the nodes $t_{n,j}$ in a manner similar to the approach described in reference (Laarabi et al. 2014). These nodes serve as quadrature points for the $(k+1)$ Guass Lobatto formula on I_n. Specifically, this yields $t_{n,0}=t_{n-1}$ and $t_{n,k}=t_n$. Next, the starting conditions for equation (15) can be seen as the same as the requirement,

$\mathbf{V}_n^0=\mathbf{v}|_{I_n-1}(t_{n-1})$ if $n\geq 2$ or $\mathbf{V}_n^0=\mathbf{v}_0$ if $n=1$

The remaining points $t_{n,1}$, $t_{n,2}\cdots$, $t_{n,k}$ are selected as the quadrature points of a k-point Gaussian formula on I_n. This formula is precise when the function being integrated is a polynomial with a degree that is less than or equal to $2k-1$, as shown in representation (16). Now, we establish the basis function $\varphi_{n,j}$ using an affine reference transformation, i.e. $T_n:\hat{I}\to I_n$ with $\hat{I}=[-1,1]$ and

$$t=T_n(\hat{t})=\frac{t_{n-1}+t_n}{2}+\frac{\tau_n}{2}\hat{t}\in I_n\qquad\hat{t}\in\hat{I},n=1,\ldots,N.\tag{19}$$

Let $\hat{\boldsymbol{\phi}}_j\in\mathbb{M}_k(\hat{I})$ denote the basis functions which satisfying the following conditions

$$\hat{\boldsymbol{\phi}}_j(\hat{t}_i)=\delta_{i,j},\quad i,j=0,\ldots,k,$$

where $\hat{t}_i$ represents the quadrature points for $\hat{I}$.

Using this, we establish the fundamental functions on I_n through the standard mapping

$$\phi_{n,j}(t) = \hat{\phi}_j(\hat{t}) \text{ with } \hat{t} = T_n^{-1}(t) = \frac{2}{\tau_n}(t - \frac{t_{n-1} + t_n}{2}) \in \hat{I}.$$

By the same way, we define the test basis function $\Omega_{n,i}$ by employing an appropriate reference basis function $\hat{\Omega}_i \in \mathbb{M}_{k-1}(\hat{I})$, i.e.

$$\Omega_{n,i}(t) = \hat{\Omega}_i(T_n^{-1}(t)) = \hat{\Omega}_i(\hat{t}), \qquad t \in I_n, i = 1, \ldots, k.$$

From Equation (17), we get for $\mathbf{v}'_\tau$,

$$\mathbf{v}'_\tau(t) = \sum_{j=0}^{k} \mathbf{V}_n^j \phi'_{n,j}(t), \qquad t \in I_n, \tag{20}$$

which leads, for each test basis function Ω and $v \in \mathbf{V}$ to a formula

$$\int_{I_n} \langle \mathbf{v}'_\tau(t), v\rangle \Omega(t)dt = \sum_{\eta=0}^{k} \hat{\rho}_\eta \sum_{j=0}^{k} \langle \mathbf{V}_n^j, v\rangle \hat{\phi}'_j(\hat{t}_\eta)\hat{\Omega}'(\hat{t}_\eta). \tag{21}$$

At last, we arrive at the specific formulation of the numerically integrated I_n-problem of cGP(k) when we choose a test function $\Omega_{n,i} \in \mathbb{M}_{k-1}(I_n)$ such that

$$\hat{\Omega}_i(\hat{t}_\eta) = (\hat{\rho}_\eta)^{-1}\delta_{i,\eta}, \qquad i, \eta = 1, \ldots, k.$$

The result of the above computation is a non-linear $(k \times k)$-block system with $V_n^0 = v_{n-1}^-$ as the initial value to find the solutions $V_n^j \in V, j = 1, \ldots, k$ which is,

$$\sum_{j=0}^{k} \gamma_{i,j}\mathbf{V}_n^j = \frac{\tau_n}{2}\{G(t_{n,i}, \mathbf{V}_n^i) + \beta_i G(t_{n,0}, \mathbf{V}_n^0)\}, \quad i = 1, \ldots, k. \tag{22}$$

where $\gamma_{i,j}$ and β_i are defined as:

$$\gamma_{i,j} = \hat{\phi}_j{}'(\hat{t}_i) + \beta_i \hat{\phi}_j{}'(\hat{t}_0), \qquad \beta_i = \hat{\rho}_0\hat{\Omega}_i(\hat{t}_0). \tag{23}$$

The importance of utilizing Lagrange basis function $\phi_{n,j}$ in relation to certain points $t_{n,j} \in \tilde{I}_n$ is that the coefficients $\mathbf{V}_n^j \in \mathbf{V}$ have the meaning $\mathbf{V}_n^j = v_\tau(t_{n,j})$.

Now, we will explore the approach for the cases $k = 1$ and $k = 2$ in the following two subsections:

3.1. cGP(1)-method

We utilize the 2-point Gauss-Lobatto formula, employing equal weights $\hat{\rho}_0 = \hat{\rho}_1 = 1$ and quadrature points $t_{n,0} = t_{n-1}, t_{n,1} = t_n$ that are positioned next to one another. This formula leads to the Trapezoidal rule. Upon careful analysis, it is determined that $\gamma_{1,0} = -1$, $\gamma_{1,1} = 1$, and $\tau_1 = 1$. This problem results in the following block-equation for the single coefficient. $\mathbf{V}_n^1 = \mathbf{v}_\tau(t_n) \in \mathbf{V}$

$$\mathbf{V}_n^1 - \mathbf{V}_n^0 = \frac{\tau_n}{2}\{G(t_n, \mathbf{V}_n^1) + G(t_{n-1}, \mathbf{V}_n^0)\}. \tag{24}$$

3.2. cGP(2)-method

We now apply the appropriate weights to the 3-point Gauss-Lobatto formula. All three of the values of $\hat{\rho}_0$, $\hat{\rho}_2$, and $\hat{\rho}_1$ are exactly fractions. Using the same values, the quadrature points $t_{n,0}$, $t_{n,1}$, and $t_{n,2}$ are also found. In this particular arrangement, Simpson's rule is applied. We then computed the coefficients.

$$\gamma_{i,j} = \begin{bmatrix} \frac{-5}{4} & 1 & \frac{1}{4} \\ 2 & -4 & 2 \end{bmatrix}, \qquad \beta_i = \begin{bmatrix} \frac{1}{2} \\ 1 \end{bmatrix}, \quad i = 1, 2, \quad \text{and} \quad j = 0, 1, 2. \tag{25}$$

We must figure out two unknown functions $\mathbf{V}_n^j = \mathbf{v}_\tau(t_{n,j})$ on the time interval $I_n = (t_{n-1}, t_n]$ with $t_{n,j} = T_n(\hat{t}_j)$ for $j = 1, 2$. We will get the following coupled (2×2)-block system for $\mathbf{V}_n^1, \mathbf{V}_n^2 \in \mathbf{V}$ which is,

$$\begin{aligned} \mathbf{V}_n^1 + \tfrac{1}{4}\mathbf{V}_n^2 &= \tfrac{5}{4}\mathbf{V}_n^0 + \tfrac{\tau_n}{2}\{G(t_{n,1}, \mathbf{V}_n^1) + \tfrac{1}{2}G(t_{n,0}, G_n^0)\}, \\ -4\mathbf{V}_n^1 + 2\mathbf{V}_n^2 &= -2\mathbf{V}_n^0 + \tfrac{\tau_n}{2}\{G(t_{n,2}, \mathbf{V}_n^2) - G(t_{n,0}, G_n^0)\}. \end{aligned} \tag{26}$$

3.3. Numerical results

Here, we utilized the cGP(2)-method for determining the numerical solution of the SIR model. We demonstrate the effect of altering the values for different model parameters while keeping the values for other parameters constant. We comprehended the behaviour and consequences of the various factors by visualizing the information. From graphs, it can be seen that dynamical behaviour of S(t), I(t), $R(t)$ has been changed with the change in the values of parameters. The analysis is based on how does the behaviour of an equilibrium solution change when the value of parameters are changed. We notice only the cases when value of a single parameter is changed and other keep fixed. Analysis of model is made numerically which is based on the previous results. For the numerical solutions of model we used the standard values of parameters given in the Table 1. The effects of μ (natural death rate) of population on susceptible, infected and recovered individuals are represented in Figures 1–3. Figure 1 shows that when we increase the natural death rate, susceptible individuals decrease and become stable after three weeks approximately. The behaviour of infected individuals shown in Figure 2. From Figure 2 we observed that increase in the value of μ has a significant decline in infected individuals population graph. For different values of μ clear change appeared in the infected population and became stable at different stages. Similar effects of μ on recovered individuals shown in Figure 3. The parameter λ denotes the rate of effective contact between susceptible and infected individuals. This represents how fast susceptible become infected. It could be seen by comparison of Figures 4 and 5 that susceptible individuals decrease while infected individuals increase when we increase the value of λ. The effects of λ on recovered individuals shown in Figure 6, recovered individuals increase by increasing the value of λ. For different values of λ, this part of population becomes stable after the second week approximately. The parameter γ_1 shows the recovery rate of infected individuals. Variational effects of γ_1 shown in the Figures 7–9 for susceptible, infected and recovered individuals, respectively. This parameter has worthy effect on infected and recovered individuals as compared to susceptible. It can be seen from Figure 8 that increase in the value of γ_1 decreases the infected individuals and they become recovered sharply. Based on the data

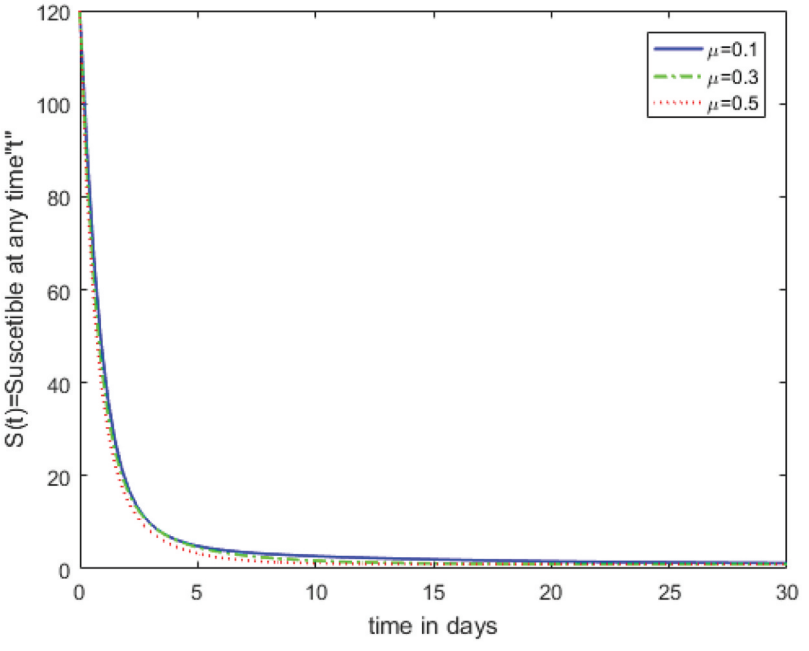

Figure 1. The impact of μ on the overall dynamics of susceptible individuals.

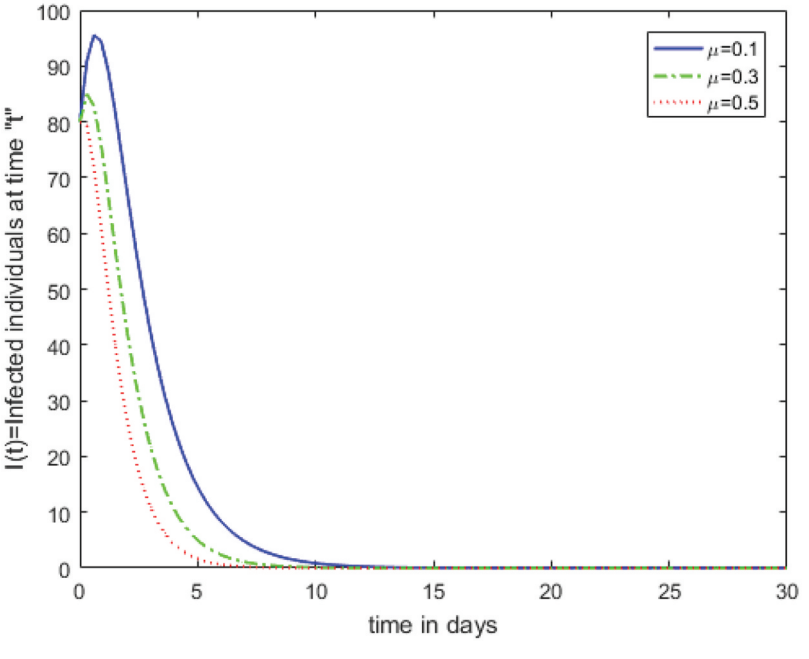

Figure 2. The significance of μ on the population dynamics of infected individuals.

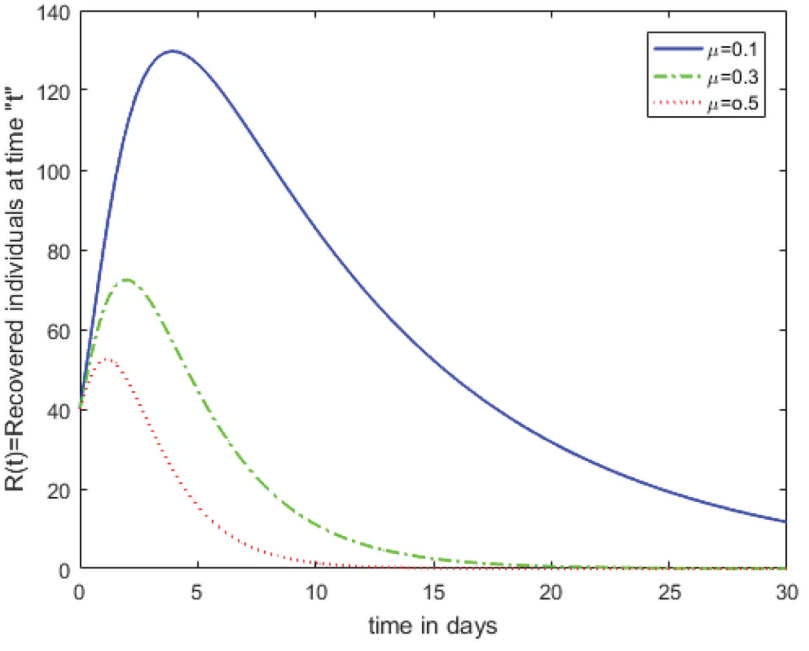

Figure 3. The implications of μ on the population dynamics of recovered individuals.

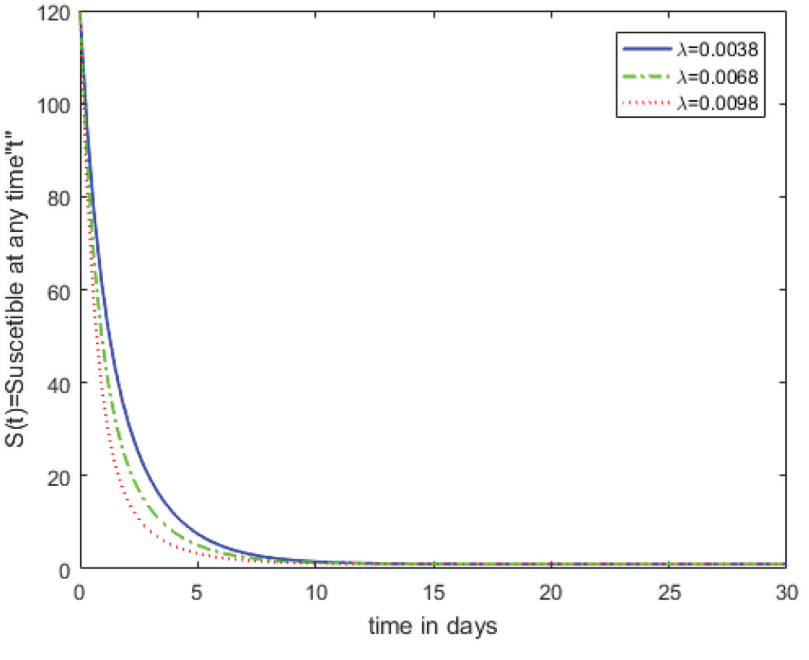

Figure 4. The effect of λ on population dynamics of susceptible individual.

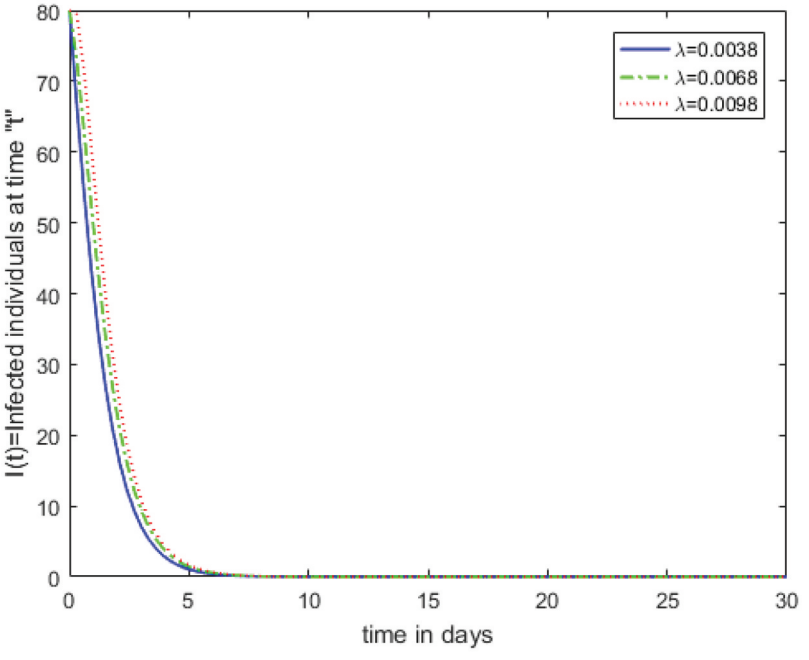

Figure 5. The effect of λ on population dynamics of infected individual.

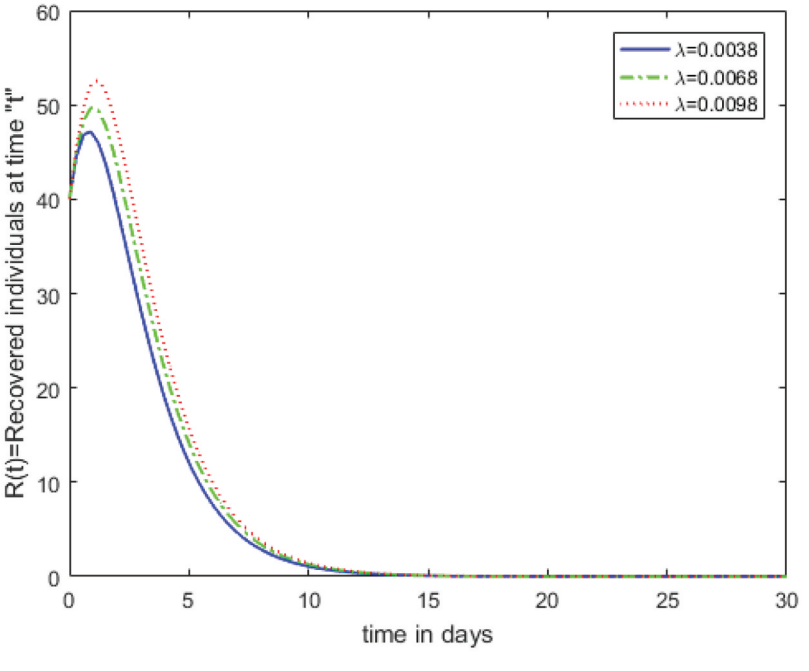

Figure 6. The effect of λ on population dynamics of recovered individual.

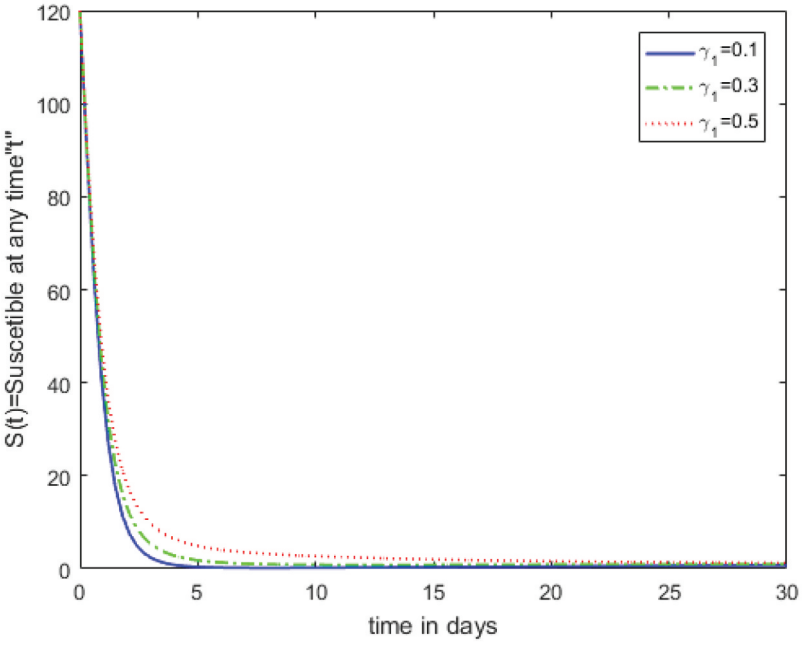

Figure 7. The influence of γ_1 on susceptible individual.

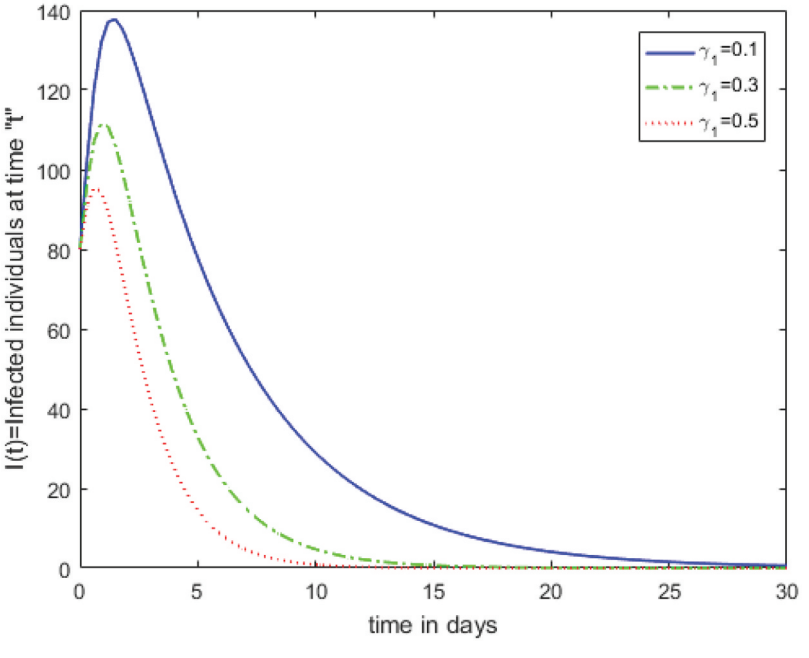

Figure 8. The influence of γ_1 on infected individual.

presented in Figure 8, it is clear that there is a significant rise in the number of infected individuals within the initial five days approximately as the value of γ_1 increases. The increment in the value of γ_1 decreases the infected individuals and they become stable earlier.

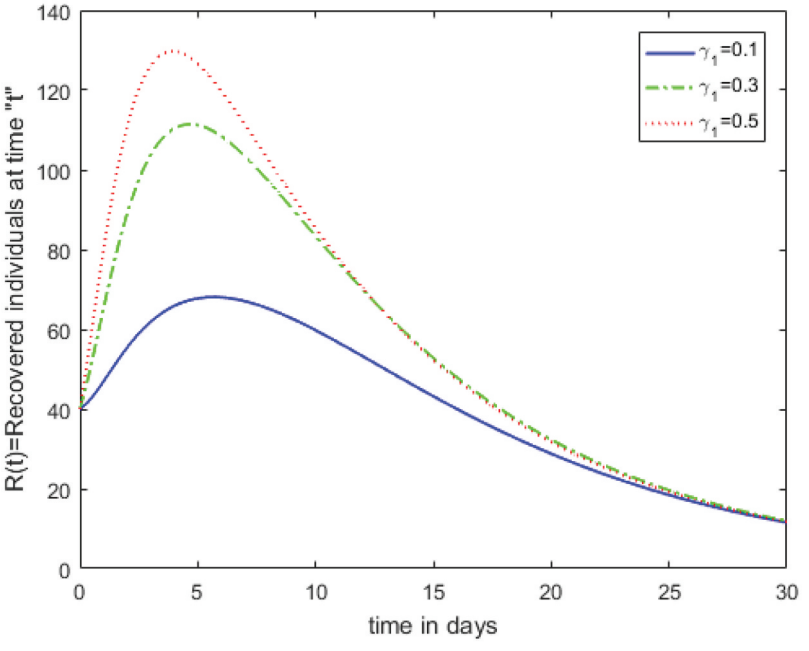

Figure 9. The influence of γ_1 on recovered individual.

Consequently, recovered individuals got individuals from infected part of population due to higher recovery rate and increased their population significantly. This observation guides that high level of recovery rate would decrease the infection. Biologically, such type of medicines can be helpful infected individuals whose recovery rate is high. This type of medication immunes the infected individuals to become recovered.

4. The solution of SIR model with vaccination, treatment and incidence rates

In this section, we intend on examining the enhancement of the SIR model introduced by Romanullah and Islam (2013). The numerical solutions are obtained using the cGP(2)-method. The graphs of the model for susceptible, infected, and recovered individuals have been displayed to provide insight into the impact of various parameters and to better understand the behaviour of the model.

4.1. Modified model

This section deals with the development of the novel model by including nonlinear incidence rate $\frac{\beta SI}{1+\alpha I}$ considered by Altaf et al. (2015). We also introduced vaccination $u_1(t)$ and treatment $u_2(t)$ rates (for more details see (Cebeci et al. 2005; Zaman et al. 2008; Wan and Cui 2009; Hussain 2011; Kongnuy and Pongsumpun 2011; Kongnuy et al. 2011; Fathalla et al. 2012; Yusuf and Benyah 2012; Altaf et al. 2015; Khalid et al. 2015; Naz et al. 2015). The extended model is as follows:

$$\begin{aligned}
\frac{dS}{dt} &= \mu - \lambda S(t)I(t) - \mu S(t) - u_1(t)S(t) - \frac{\beta SI}{1+\alpha I},\\
\frac{dI}{dt} &= \frac{\beta SI}{1+\alpha I} + \lambda S(t)I(t) - \gamma_1 I(t) - \mu I(t) - u_2(t)I(t),\\
\frac{dR}{dt} &= \gamma_1 I(t) - \mu R(t) + u_1(t)S(t) + u_2(t)I(t).
\end{aligned} \tag{27}$$

The disease-free equilibrium points are characterized by the absence of any disease. To achieve disease-free equilibrium points, we established the initial conditions as follows: $S(0) = S_0$ and $I(0) = 0$, $R(0) = 0$. To examine the dynamic behaviour of the equations (27), we formulate the right-hand side of each equation equal to zero. We may formulate the first equation from (27) as follows:

$$\mu - \lambda S(t)I(t) - \mu S(t) - u_1(t)S(t) - \frac{\beta SI}{1+\alpha I} = 0. \tag{28}$$

By using initial conditions, we obtained by direct calculations a disease free point which is $S_0 = \frac{\mu}{\mu+u_1}$.

4.2. Sensitivity analysis

We perform a sensitivity analysis of the reproduction number in order to ascertain the effect of the incorporated parameter on R_0. We use well-known methods such as Partial Rank Correlation Coefficient ($\mathbb{PRCC}$) and Latin Hypercube Sampling ($\mathbb{LHS}$) to ascertain the impact of the associated characteristics. Using this procedure, we obtain $\mathbb{PRCC}$ and p-values for every variable and perform a significance assessment. Regardless of the sign, lesser p-values and higher $\mathbb{PRCC}$ values indicate the more sensitive aspects of the system.

The $\mathbb{PRCC}$ test results are illustrated in the Figure 10. The $\mathbb{PRCC}$ values are $\mu = -0.8941$, $\lambda = 0.9277$, $\gamma_1 = 0.8171$, $\beta = -0.0269$, $\alpha = 0.0749$, $\mu_1 = -0.0527$,

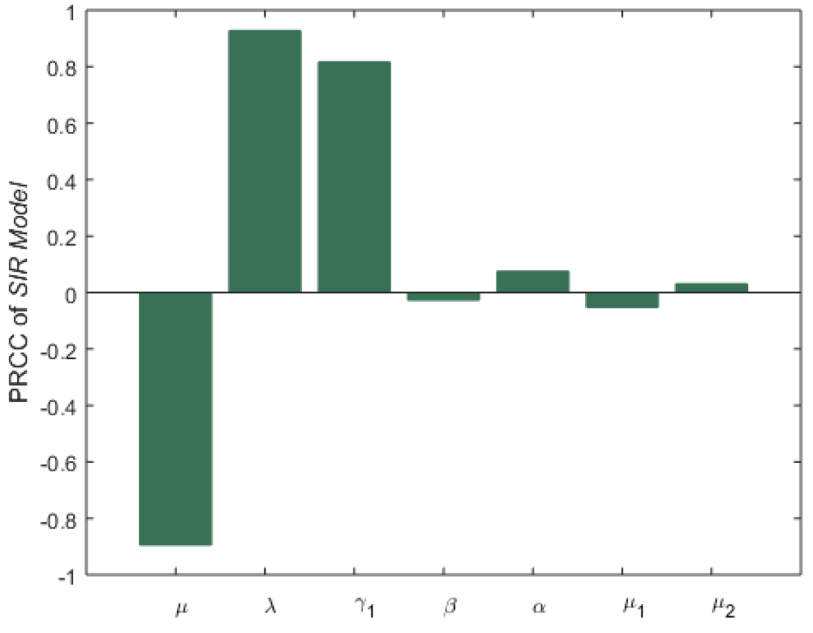

Figure 10. Plotting sensitivity ratings versus parameters in a histogram.

$\mu_2 = 0.0304$, while the p values are $\mu = 0.0000$, $\lambda = 0.0000$, $\gamma_1 = 0.0000$, $\beta = 0.3970$, $\alpha = 0.0182$, $\mu_1 = 0.0965$, $\mu_2 = 0.3389$. We noticed that the parameters μ, β, and μ_1 are the most sensitive factors of the basic reproduction number R_0. It is therefore advised that health professionals consider these worries. The $\mathbb{PRCC}$ findings are represented in Figure 10.

4.3. Numerical simulations and discussions

In this section of the manuscript, we utilize the cGP(2) method to analyse the SIR model described by Equation 27 to acquired the numerical solutions for the innovative SIR model. The values of different parameters and variables are listed in Table 1. In order to analyze the impact of different parameters, we make adjustments to certain variables while keeping the rest constant. Figure 14 demonstrates the effects of vaccination on individuals who are susceptible. This figure illustrates the correlation between the rate of vaccination and the ability of susceptible individuals to combat diseases. Throughout time, this capability gradually diminishes. From Figure 12, it is visible that in the initial ten days, there is a noticeable decline in the number of susceptible individuals, reaching its lowest point. As time goes by, the immune system becomes more active and resilient, leading to a stronger chance of recovery. Figure 12 illustrates that the rate of vaccination does not have an impact on the number of infected individuals. The reason for the infected individual's lack of vaccination resulted in their current condition. In addition consequence, they did not receive vaccination and the vaccination rates stayed unchanged. Figure 13 demonstrates the impact of vaccination on individuals who have recovered. The figure shown in Figure 13 illustrates how an increase in vaccination rates leads to a higher number of individuals recovering from the illness. This is because vaccinations help protect susceptible individuals and reduce the overall number of infections. These findings indicate that a higher number of individuals can be successfully

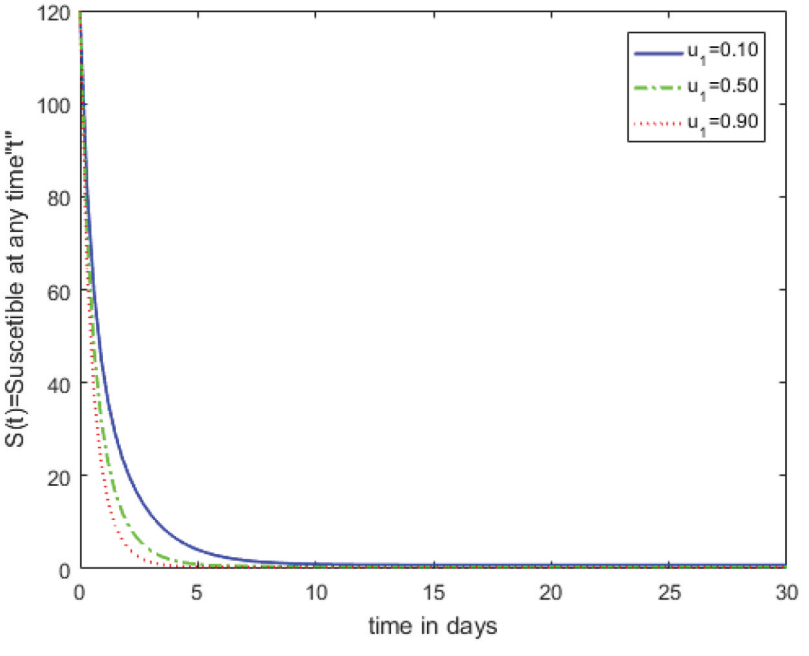

Figure 11. The concentration of u_1 on susceptible individual.

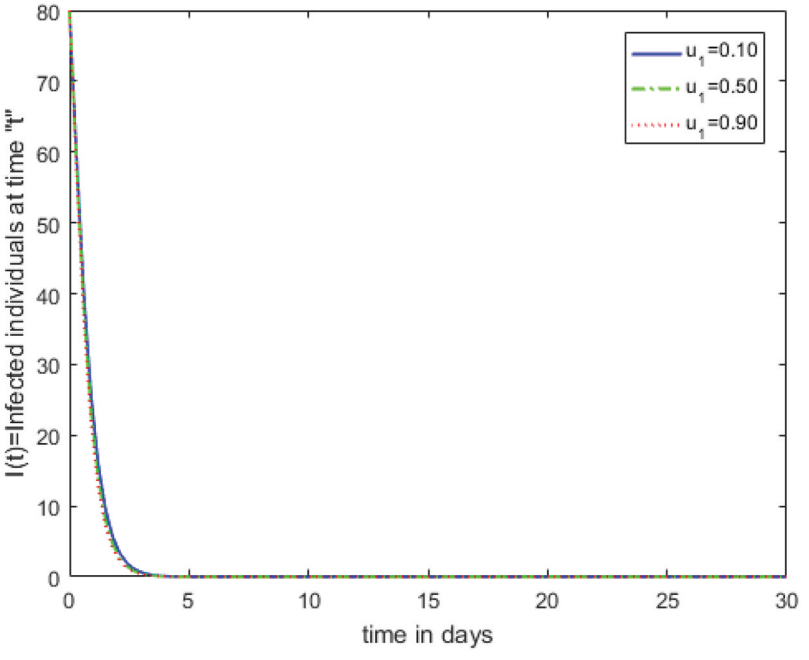

Figure 12. The concentration of u_1 on infected individual.

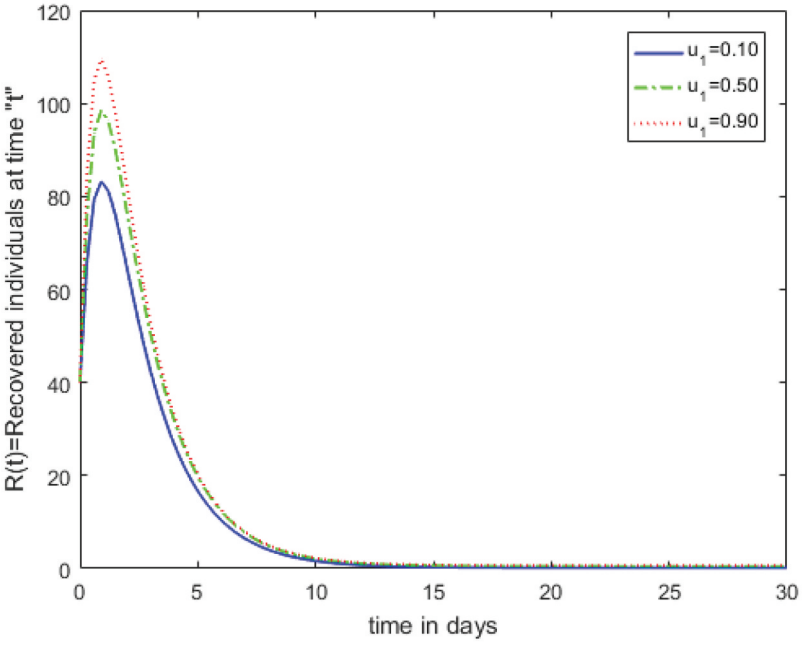

Figure 13. The concentration of u_1 on recovered individual.

recovered as a result of an increase in the vaccination rate. Figure 14 illustrates the impact of treatment rate on the susceptible population. Since the treatment rate has changed, the results remain unaffected even though the susceptible population is not receiving treatment. From Figure 15, it can be observed that an increase in the treatment rate leads to a sharp decrease in the infected population, eventually converging to the number of recovered individuals. It is

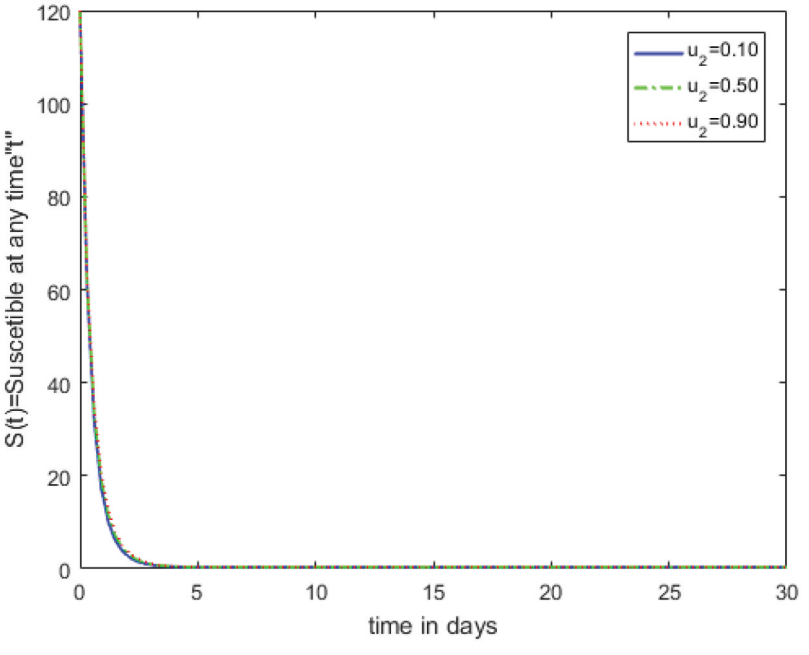

Figure 14. The influence of u_2 on the amount of susceptible individual.

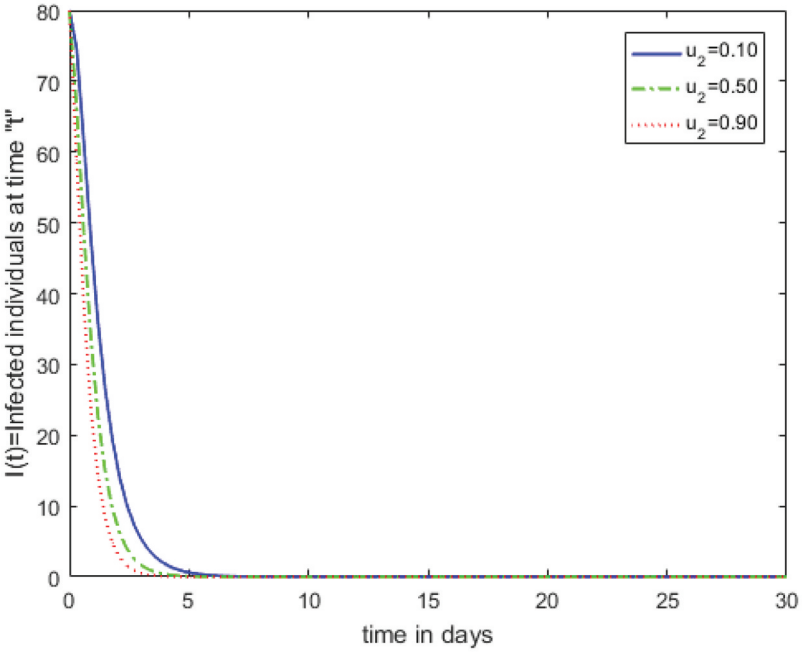

Figure 15. The influence of u_2 on the amount of infected individual.

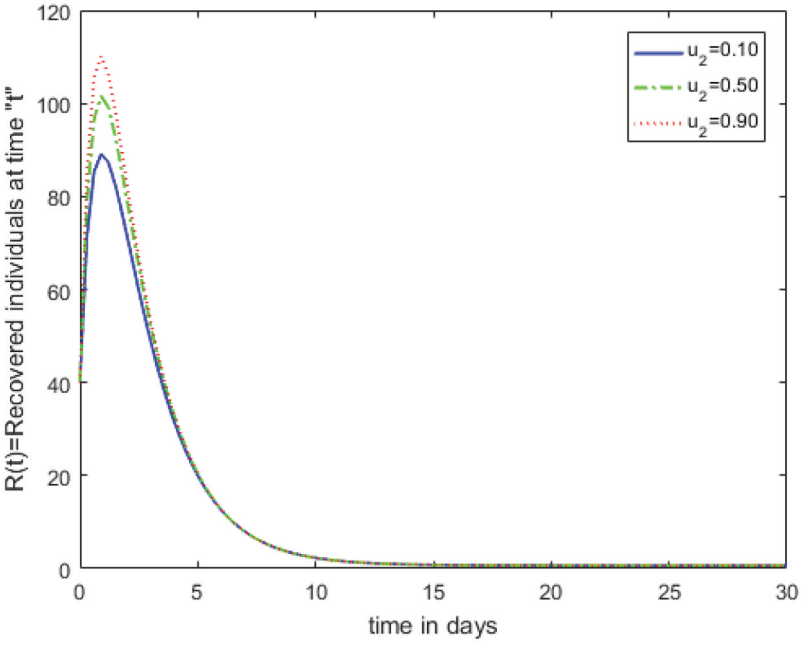

Figure 16. The influence of u_2 on the amount of recovered individual.

evident that the number of infected individuals decreases during the first week for various treatment rates. As the treatment rate increases, the infected population rapidly decreases and eventually converges to the recovered population. Figure 16 illustrates the positive impact of treatment on the infected individuals, leading to their prompt recovery. Meanwhile, the population is experiencing a rapid increase. By comparing Figures 15 and 16, it can be deduced that changes in the vaccination rate result in the emergence of new individuals who have recovered.

4.4. Combined vaccination and treatment strategy

The effects of vaccination and treatment are observed in both individuals who are susceptible to infection and those who are already infected. Figures 11–16 demonstrate the vaccination and treatment strategy, where we employ a combination of vaccination and treatment controls with varying values to reduce the number of susceptible and infected individuals. It is evident that there has been a significant reduction in the number of susceptible and infected individuals through the implementation of a combined vaccination and treatment strategy.

4.5. Only treatment control $u_1 = 0$

Figures 17–19 illustrate the effects of treatment control on individuals who are susceptible, infected, and recovered. For this, we set the vaccination control u_1 to zero while taking into account the incidence rate. Figure 18 depicts a significant decrease in the number of infected individuals. Figure 18 illustrates a slight influence on the number of individuals who are susceptible. Based on Figure 19, there has been a significant increase in the number of people who have made a recovery.

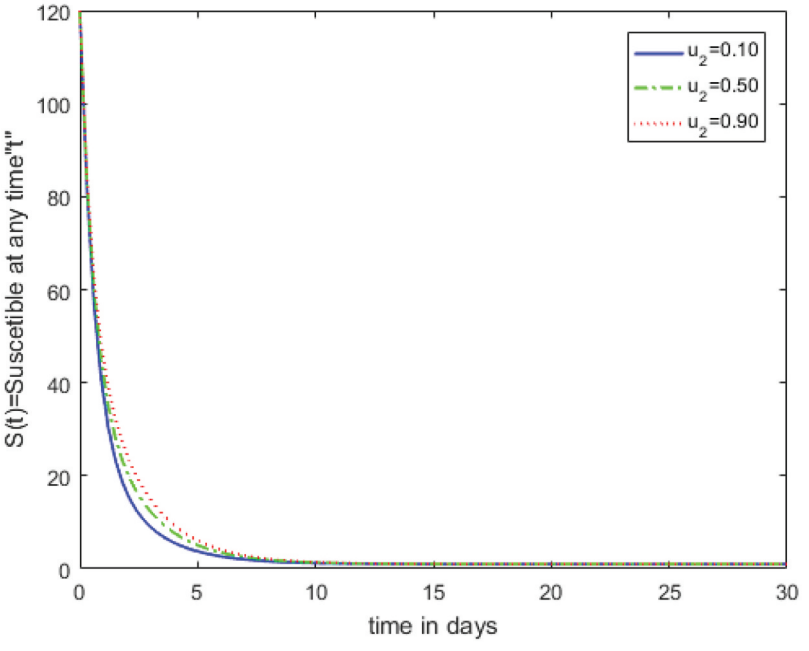

Figure 17. The impact of u_2 with $u_1 = 0$ on susceptible individual population.

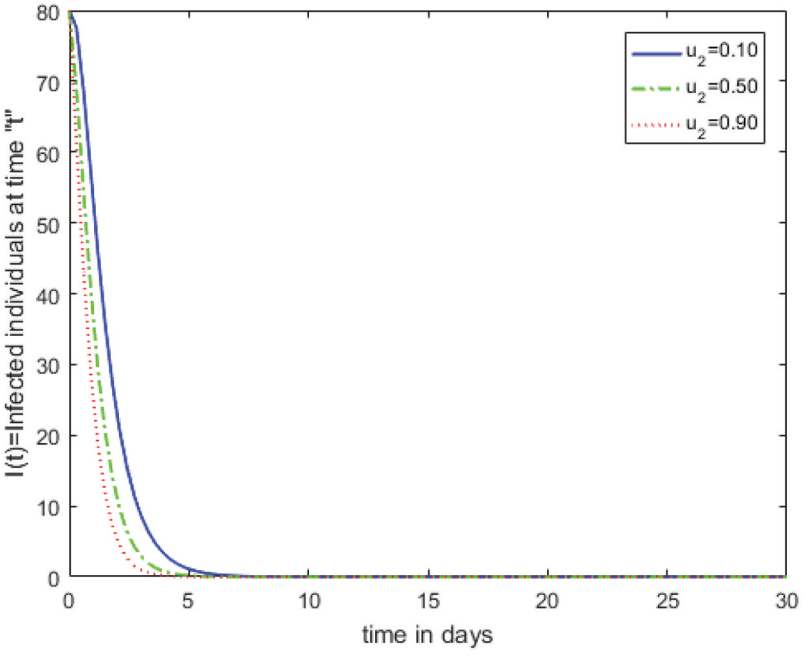

Figure 18. The impact of u_2 with $u_1 = 0$ on infected individual population.

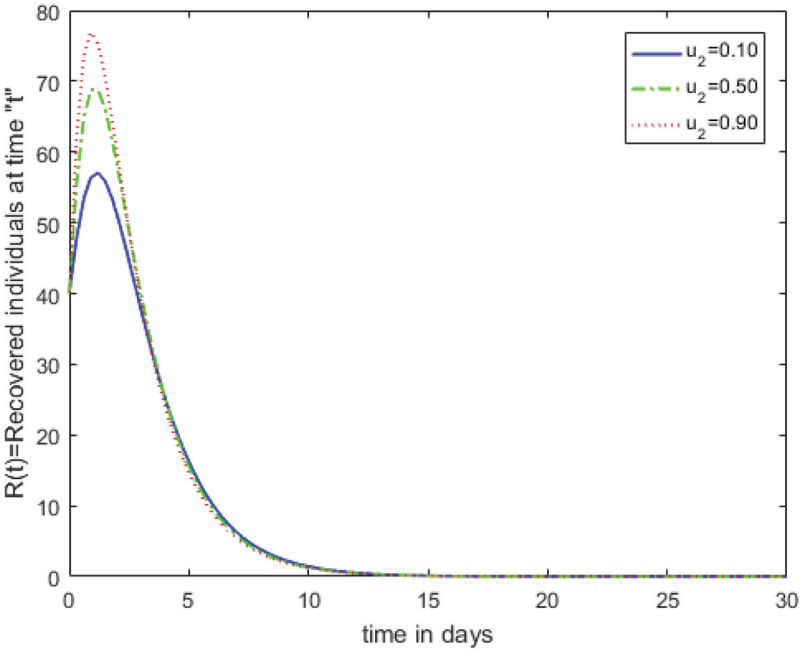

Figure 19. The impact of u_2 with $u_1 = 0$ on recovered individual population.

4.6. Only vaccination control $u_2 = 0$

Figures 20–22 provide a detailed explanation of how vaccination control impacts the population of susceptible, infected, and recovered individuals. By employing this strategy, the priority is solely on utilizing vaccination control to reduce the number of susceptible individuals and

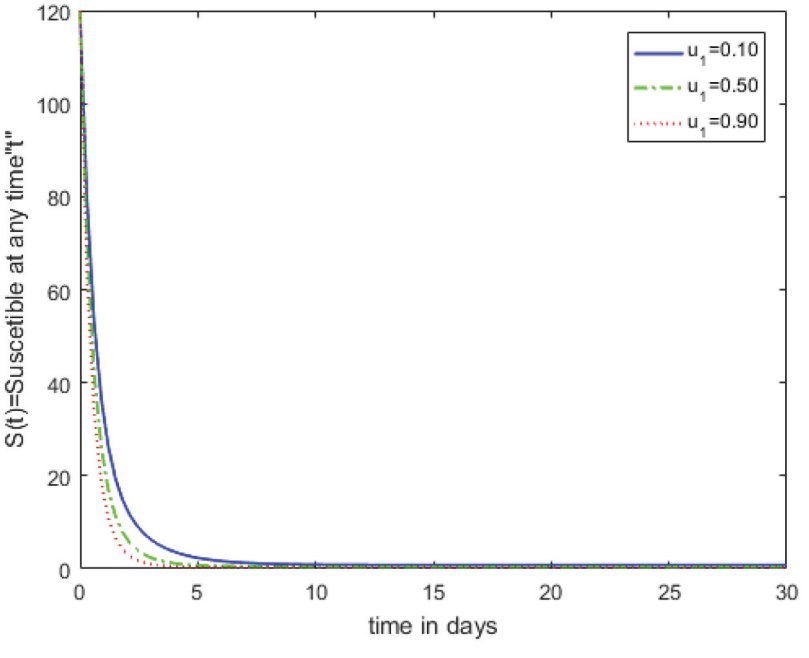

Figure 20. The effect of u_1 with $u_2 = 0$ on susceptible individual population.

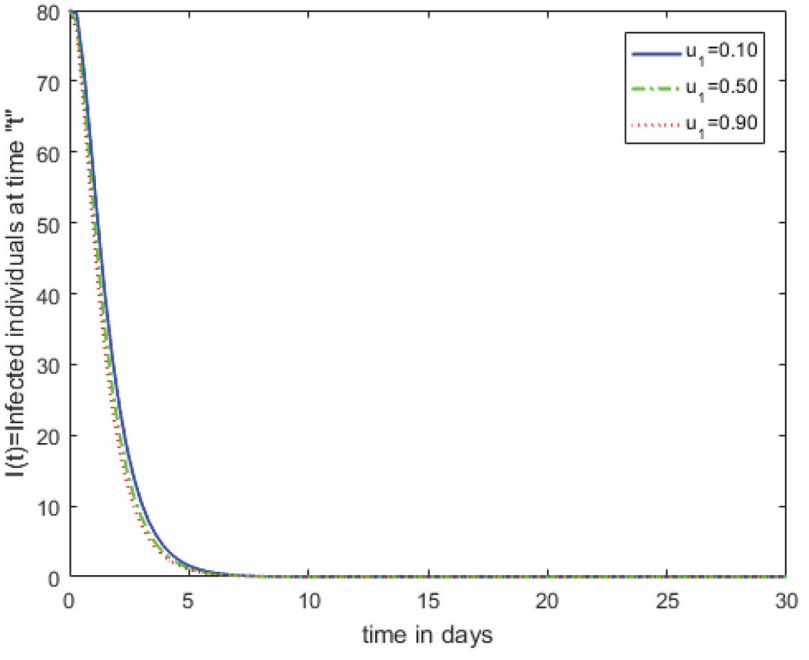

Figure 21. The effect of u_1 with $u_2 = 0$ on infected individual population.

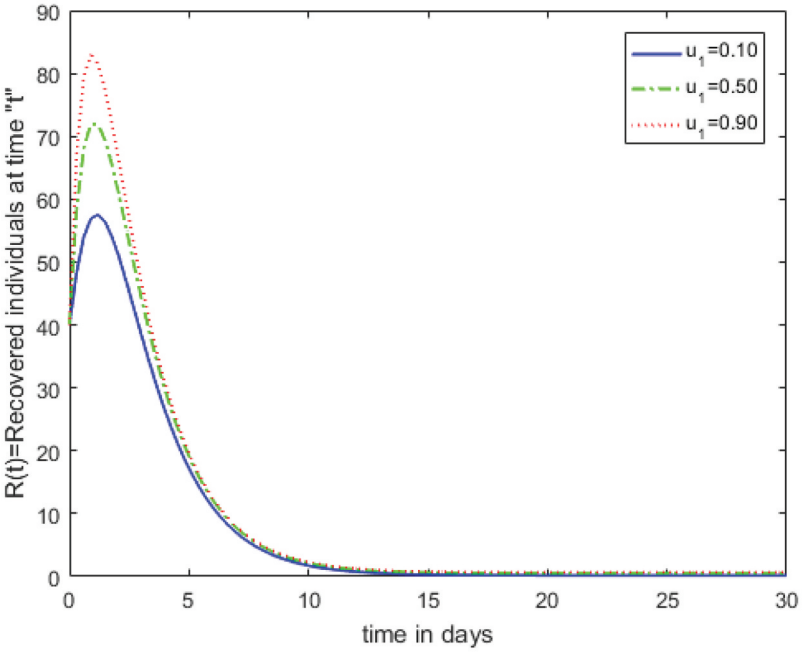

Figure 22. The effect of u_1 with $u_2 = 0$ on recovered individual population.

the incidence rate. Meanwhile, treatment control u_2 is set to zero. In Figure 20, there is a noticeable reduction in the number of individuals susceptible to the disease following vaccination. We have noticed a slight decline in the number of people who have been infected, along with a notable rise in the number of individuals who have recovered.

5. Evaluation of the RK-4 approach and the cGP(2) strategy for extended model

In this section, we delve into the solution of the extended SIR model using the Runge-Kutta method of order, specifically, the RK-4 method. Furthermore, it involves a thorough analysis of the findings in relation to the results achieved through the cGP (2)-method. The cGP(2) method has been widely recognized for its exceptional effectiveness and precision. The computer code is written in MATLAB for the determination of results. According to the data provided in the Tables 2–5, it is noticeable that the

Table 2. Comparison of the RK4 and cGP(2) methods for *S(t)*.

t_i	cGP(2)-Method	RK4-Method
0.0	1.200000000000000E + 02	1.200000000000000E + 02
0.1	0.959365757903899E + 02	0.959369480963414E + 02
0.2	0.772862610235222E + 02	0.772868213043125E + 02
0.3	0.627627291277093E + 02	0.627633634772335E + 02
0.4	0.513715650321100E + 02	0.513722080035038E + 02
0.5	0.423609844964566E + 02	0.423616008811086E + 02
0.6	0.351688696717114E + 02	0.351694421657838E + 02
0.7	0.293763585519745E + 02	0.293768801236524E + 02
0.8	0.246708050443067E + 02	0.246712744007013E + 02
0.9	0.208176387017762E + 02	0.208180576435043E + 02
1.0	0.176395520373138E + 02	0.176399239258400E + 02

Table 3. Evaluation of the cGP(2) and RK4 methods for *I(t)*.

t_i	cGP(2)-Method	RK4-Method
0.0	0.800000000000000E + 02	0.800000000000000E + 02
0.1	0.728448292670138E + 02	0.728445016464407E + 02
0.2	0.649634477930045E + 02	0.649629965414385E + 02
0.3	0.570059403325728E + 02	0.570054849128594E + 02
0.4	0.493954672300226E + 02	0.493950683657630E + 02
0.5	0.423775211548057E + 02	0.423772031779310E + 02
0.6	0.360705853367663E + 02	0.360703519256894E + 02
0.7	0.305084726764595E + 02	0.305083168761523E + 02
0.8	0.256722128964564E + 02	0.256721231099928E + 02
0.9	0.215125574052038E + 02	0.215125207903048E + 02
1.0	0.179651145390871E + 02	0.179651188112565E + 02

Table 4. Comparison of the RK4 and cGP(2) methods for *R(t)*..

t_i	cGP(2)-Method	RK4-Method
0.0	0.400000000000000E + 02	0.400000000000000E + 02
0.1	0.597116405226449E + 02	0.597115985826534E + 02
0.2	0.752827843346401E + 02	0.752826793855411E + 02
0.3	0.873222875866729E + 02	0.873221131490695E + 02
0.4	0.963763931193727E + 02	0.963761533806518E + 02
0.5	1.029282426920555E + 02	1.029279482678023E + 02
0.6	1.073997964470370E + 02	1.073994608791523E + 02
0.7	1.101556279218708E + 02	1.101552652175664E + 02
0.8	1.115078862013488E + 02	1.115075093237783E + 02
0.9	1.117218026790171E + 02	1.117214227634941E + 02
1.0	1.110212824486184E + 02	1.110209085127312E + 02

Table 5. The variation between the solutions obtained by the cGP(2)-method and RK4-method based on absolute errors.

t_i	$S(t)$	$I(t)$	$R(t)$
	$\lvert cGP(2) - RK4\rvert$	$\lvert cGP(2) - RK4\rvert$	$\lvert cGP(2) - RK4\rvert$
0.0	0.000000000000000E-03	0.000000000000000E-03	0.000000000000000E-03
0.1	0.372305951557905E-03	0.327620573116860E-03	0.041939991469064E-03
0.2	0.560280790296019E-03	0.451251566005340E-03	0.104949098997054E-03
0.3	0.634349524183619E-03	0.455419713432548E-03	0.174437603376987E-03
0.4	0.642971393737923E-03	0.398864259601339E-03	0.239738720921423E-03
0.5	0.616384652033730E-03	0.317976874704584E-03	0.294424253169723E-03
0.6	0.572494072429208E-03	0.233411076926870E-03	0.335567884690136E-03
0.7	0.521571677840171E-03	0.155800307226173E-03	0.362704304407657E-03
0.8	0.469356394557252E-03	0.089786463600916E-03	0.376877570488432E-03
0.9	0.418941728078437E-03	0.036614899034504E-03	0.379915522998431E-03
1.0	0.371888526160546E-03	0.004272169320529E-03	0.373935887282073E-03

results obtained from the cGP (2)-method were closely comparable to those of the RK-4 method. There is a slight variation between the solutions obtained by both schemes, with the results being approximately the same up to eight digits. Figures 23–25 display the graphs of three compartments: S(t), I(t), and $R(t)$. The figures clearly show the overlapping of the solutions obtained by both methods. We also determined the absolute error between the solutions of both schemes. The mesh grid graphs of Galerkin and RK4 schemes are presented in Figures 26–27. By evaluating the outcome of both methods, it becomes inescapable that the proposed scheme is both reliable as well as effective in revealing solutions for real-world problems.

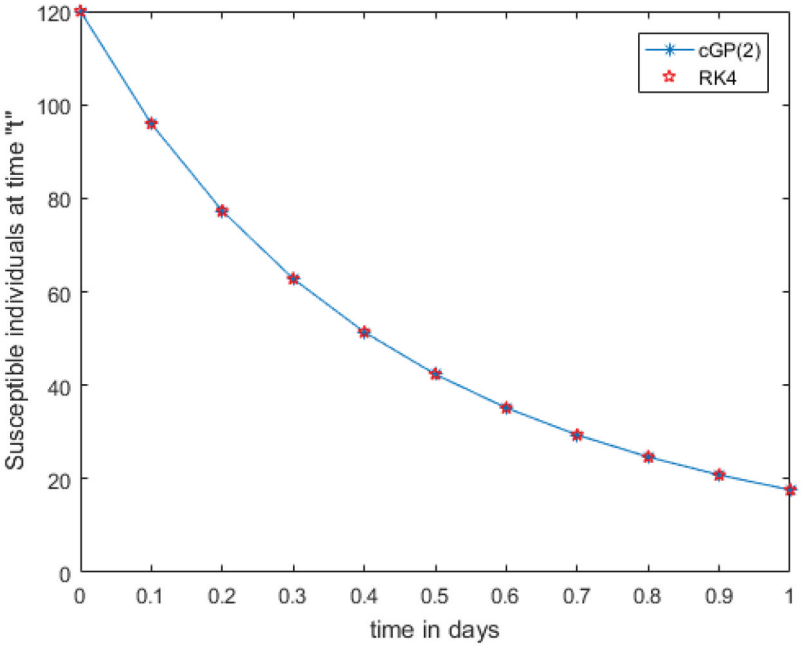

Figure 23. Graphical comparison between cGP(k)-method and RK-4 method for S(t).

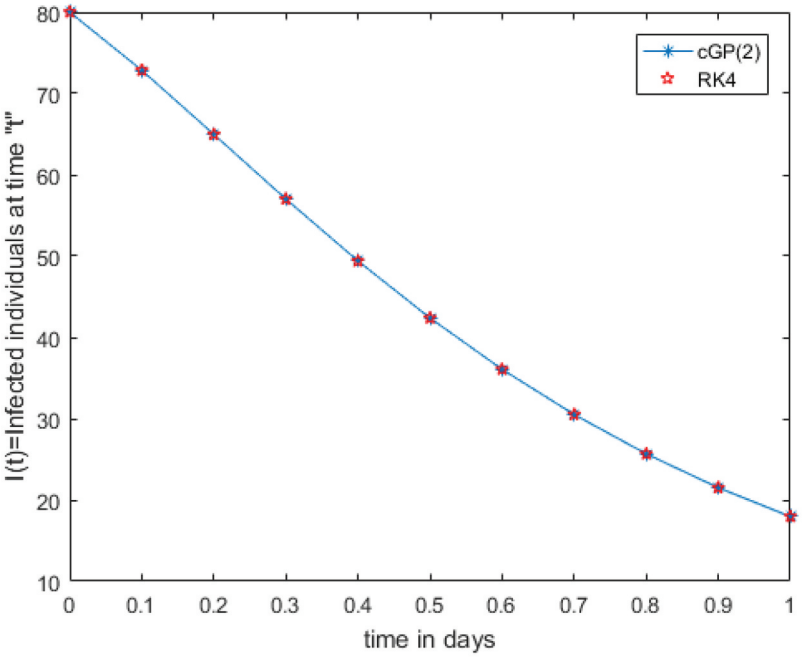

Figure 24. Graphical comparison between cGP(k)-method and RK-4 method for $I(t)$.

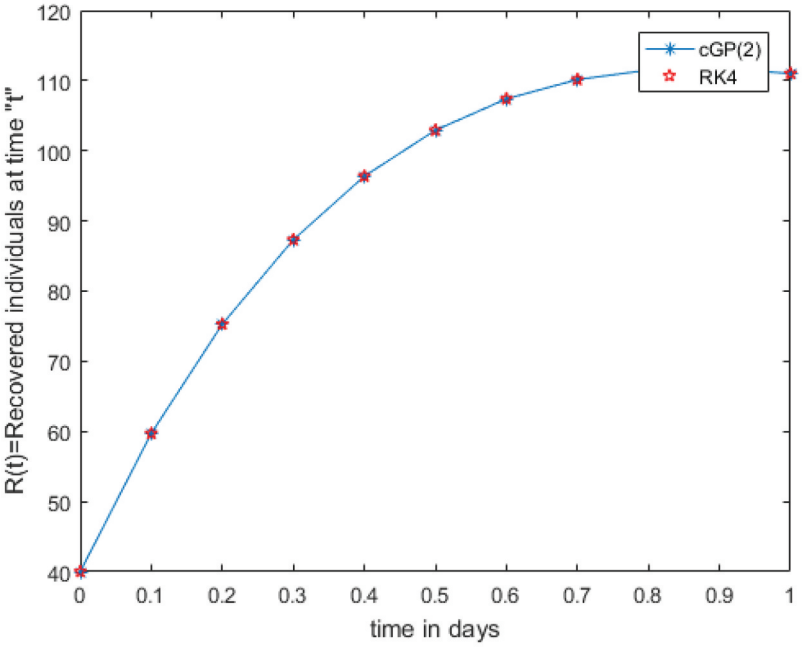

Figure 25. Graphical comparison between cGP(k)-method and RK-4 method for $R(t)$.

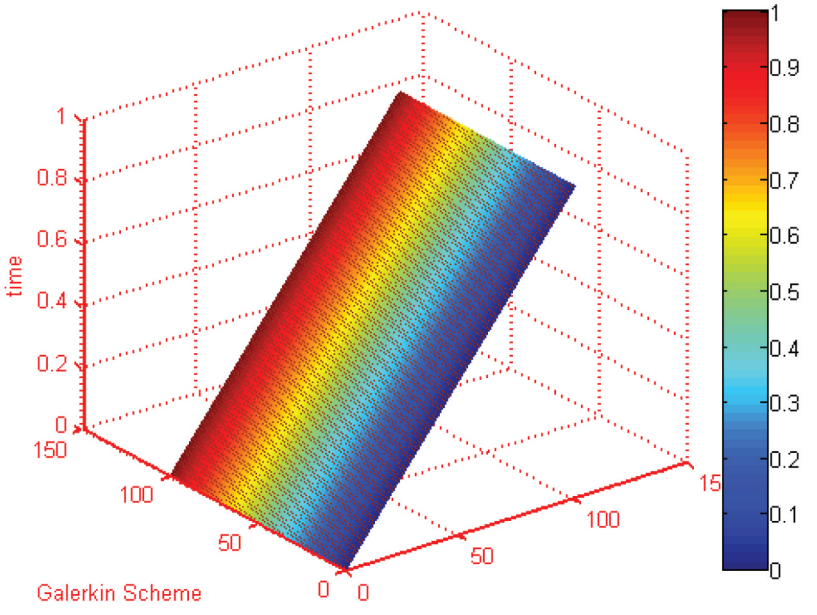

Figure 26. The mesh grid graph of Galerkin method.

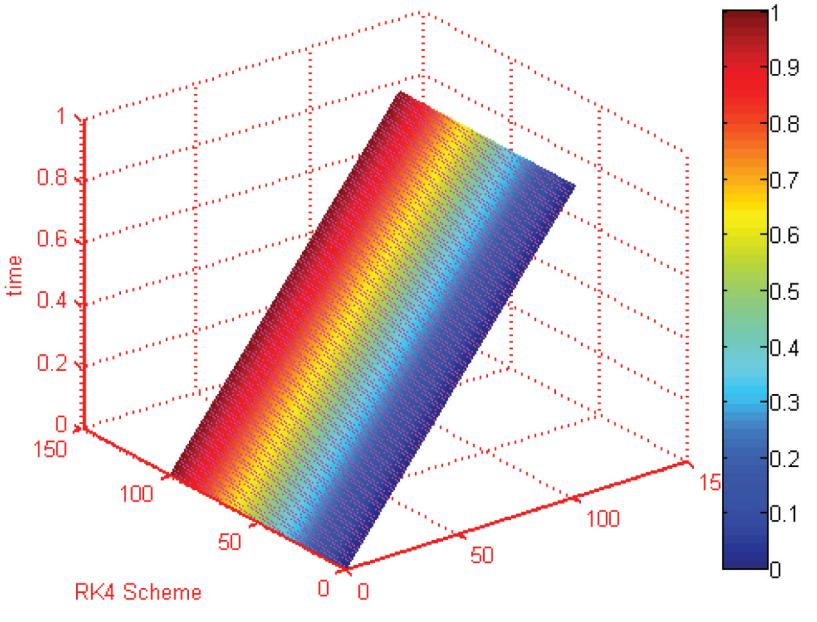

Figure 27. The mesh grid graph of RK4-method.

6. Conclusions and future recommendations

In this study, we delved into two different variations of SIR models. The model was analysed using numerical methods for determining the population of susceptible, infected, and recovered individuals for different values of the parameters involved in the model. Implementing on the widely used SIR model, an innovative approach has been developed to integrate components such as vaccination, treatment, and incidence rates. We identified the basic reproduction number, denoted as R_0, using a feasible in biology approach. We also delved into the sensitivity analysis of R_0. The solutions of both models are illustrated visually and presented in numerical representation. Based on these findings, it can be concluded that implementing vaccination and treatment control measures can effectively combat epidemics within a population. The primary objective of the current study was to establish a straightforward mathematical model that provides feasible and dependable solutions for addressing the core challenges in epidemic control. It is noted that the impact of vaccination on the population of susceptible individuals results in their exemption from their current state, leading them to converge with the recovered population. It has been determined that treatment has an impact on the population of infected individuals and leads to the recovery of individuals. The numerical solutions demonstrated the superior effectiveness of the combined vaccination and treatment control strategy. In this dissertation, the cGP(2)-method is employed to solve coupled non-linear differential equations. In terms of efficiency and precision, the present system outperforms the RK4 approach. Furthermore, the cGP(2)-method continuously outperforms the RK4-method in terms of accuracy as the number of mesh points increases. The present approach has a numerical cost similar to the RK-4 method, but it provides a greater degree of precision. Considering both approaches have the same amount of iterations in numerical solutions. The findings show that the present technique is a very effective tool for time-dependent issues, regularly producing improved approximations.

In future, we plan to implement the suggested schemes to fractional mathematical models (Ali et al. 2022; Alharbi et al. 2022; Jleli et al. 2023).

Acknowledgments

The researchers would like to thank the Deanship of Graduate Studies and Scientific Research at Qassim University for financial support (QU-APC-2024-9/1).

Disclosure statement

No potential conflict of interest was reported by the author(s).

Funding

The work was supported by The researchers would like to thank the Deanship of Graduate Studies and Scientific Research at Qassim University for financial support [QU-APC-2024-9/1].

References

Adams B, Holmes EC, Zhang C, Mammen MP, Nimmannitya S, Kalayanarooj S, Boots M. 2006. Cross-protective immunity can account for the alternating epidemic pattern of dengue virus serotypes circulating in Bangkok. Proc Natl Acad Sci USA. 103(38):14234–14239. doi: 10.1073/pnas.0602768103.

Alharbi R, Jan R, Alyobi S, Altayeb Y, Khan Z. 2022. Mathematical modeling and stability analysis of the dynamics of monkeypox via fractional-calculus. Fractals. 30(10):2240266. doi: 10.1142/S0218348X22402666.

Ali U, Naeem M, Abdullah FA, Wang MK, Salama FM. 2022. Analysis and implementation of numerical scheme for the variable-order fractional modified sub-diffusion equation. Fractals. 30 (10):2240253. doi: 10.1142/S0218348X22402538.

Altaf M, Ali Z, Dennis LCC, Khan I, Islam S, Ullah M, Gul T. 2015. Stability analysis of an SVIR epidemic model with non-linear saturated incidence rate. Appl Mathematical Sci. 9 (23):1145–1158. doi: 10.12988/ams.2015.41164.

Anderson M, May M, Anderson B. 1992. Infectious diseases of humans: dynamics and control. Vol. 28. Germany: Wiley Online Lib.

Aron J, R. Robert. 1982. The population dynamics of malaria 139–179. Chapman and Hall, London: Population Dynamics of Infectious Diseases.

Attaullah JM, Alyobi S, Yassen MF, Weera W. 2023. A higher order galerkin time discretization scheme for the novel mathematical model of COVID-19. Aims Math. 8(2):3763–3790. doi: 10.3934/math.2023188.

Attaullah RD, Weera W. 2022. Galerkin time discretization scheme for the transmission dynamics of HIV infection with non-linear supply rate. J Aims Math. 7(6):11292–11310. doi: 10.3934/math.2022630.

Attaullah YMF, Alyobi S, Al-Duais FS, Weera W. 2023. On the comparative performance of fourth order RungeKutta and the GalerkinPetrov time discretization methods for solving nonlinear ordinary differential equations with application to some mathematical models in epidemiology. Aims Math. 8(2):3699–3729. doi: 10.3934/math.2023185.

Attaullah Alyobi S, Yassen MF. 2022. A study on the transmission and dynamical behavior of an HIV/AIDS epidemic model with a cure rate. Aims Math. 7(9):17507–17528. doi: 10.3934/math.2022965.

Attaullah Jan R, YÃzbasi S, Yüzbaşı Ş. 2021. Dynamical behaviour of HIV infection with the influence of variable source term through Galerkin method. Chaos, Solitons Fractals. 152:111429. doi: 10.1016/j.chaos.2021.111429.

Attaullah Sohaib A, Sohaib M. 2020. Mathematical modeling and numerical simulation of HIV infection model. Results In Appl Math. 7:100118. doi: 10.1016/j.rinam.2020.100118.

Cebeci T, Shao JP, Kafyeke F, Laurendeau E. 2005. Computational fluid dynamics for engineers. Germany, Berlin: Springer.

Centres PM, Perez-Morelo DJ, Guzman R, Reinaudi L, Gimenez MC. 2024. Diffusion model for the spread of infectious diseases: SIR model with mobile agents. Physica A: Stat Mech Appl. 633:129399. doi: 10.1016/j.physa.2023.129399.

Classification, Medical Microbiology. 1996. Berlin, Germany; p. 213–261.

Cummings DAT, Schwartz IB, Billings L, Shaw LB, Burke DS. 2005. Dynamic effects of antibody-dependent enhancement on the fitness of viruses. Proc Natl Acad Sci USA. 102 (42):15259–15264. doi: 10.1073/pnas.0507320102.

Dat C, D. Lesser. 2013. Infectious disease dynamics. In: Nelson K Masters Williams C, editors. Infectious disease epidemiology. Burlington (MA): Jones and Bartlett Learning; p. 138–139, 830–831.

Degallier N, Favier C, Boulanger JP, Menkes C. 2009. Imported and autochthonous cases in the dynamics of dengue epidemics in Brazil. Rev Saúde Pública. 43(1):1–7. doi: 10.1590/S0034-89102009000100001.

Derouich M, Boutayeb A, Twizell EH. 2003. A model of dengue fever. Biomed Eng Online. 2(1):4. doi: 10.1186/1475-925X-2-4.

Dhahbi AB, Chargui Y, Boulaaras S, Rahali S, Mhamdi A. 2022. The proliferation of COVID-19 in Saudi Arabia according to Gompertz model. Fractals. 30(10):2240251. doi: 10.1142/S0218348X22402514.

Dietz K, Heesterbeek JA, Tudor DW. 1993. The basic reproduction ratio for sexually transmitted diseases part 2. Effects of variable HIV infectivity. Math Biosci. 117(1–2):35–47. doi: 10.1016/0025-5564(93)90016-4.

Elbasha EH and Galvani AP. 2005. Vaccination against multiple HPV types. Math Biosci. 197 (1):88–117. doi: 10.1016/j.mbs.2005.05.004.

Esteva L, Vargas C. 1998. Analysis of a dengue disease transmission model. Math Biosci. 150 (2):131–151. doi: 10.1016/S0025-5564(98)10003-2.

Esteva L, Vargas C. 2000. Influence of vertical and mechanical transmission on the dynamics of dengue disease. Math Biosci. 167(1):51–64. doi: 10.1016/S0025-5564(00)00024-9.

Fathalla A, Anwar, Rihan MN. 2012. Qualitative analysis of delayed SIR epidemic model with a saturated incidence rate. Int J Differ Equations. 2012, 1–13. Article ID 408637. doi: 10.1155/2012/408637.

Favier C, Schmit D, Muller DM, Cazelles B, Degallier N, Mondet B, Dubois MA. 2005. Influence of spatial heterogeneity on an emerging infectious disease: the case of dengue epidemics. Proc R Soc B. 272(1568):1171–1177. doi: 10.1098/rspb.2004.3020.

Feng Z, Hernandez JX. 1997. Competitive exclusion in a vector-host model for the dengue fever. J Math Biol. 35(5):523–544. doi: 10.1007/s002850050064.

Focks DA, Daniels E, Haile DG, Keesling JE. 1995. A simulation model of the epidemiology of urban dengue fever: literature analysis, model development, preliminary validation, and samples of simulation results. Am J Trop Med Hyg. 53(5):489–506. doi: 10.4269/ajtmh.1995.53.489.

Hu Z, Ma W, Ruan S. 2012. Analysis of SIR epidemic models with nonlinear incidence rate and treatment. Math Biosci. 238(1):12–20. doi: 10.1016/j.mbs.2012.03.010.

Hussain S. 2011. A note on accurate and efficient higher order galerkin time stepping schemes for the nonstationary stokes equations. Open Numer Methods J. 4(1):35–45. doi: 10.2174/1876389801204010035.

Hussain S, Schieweck F, Turek S. 2011. Higher order galerkin time discretization and fast multigrid solvers for the heat equation. J Numer Math. 19(1):41–61. doi: 10.1515/jnum.2011.003.

Jan R, Boulaaras S, Alyobi S, Rajagopal K, Jawad M. 2023. Fractional dynamics of the transmission phenomena of dengue infection with vaccination. Discrete Contin Dyn Syst Ser S. 16(8):2096–2117. doi:10.3934/dcdss.2022154.

Jan R, Qureshi S, Boulaaras S, Pham VT, Hincal E, Guefaifia R. 2023. Optimization of the fractional-order parameter with the error analysis for human immunodeficiency virus under Caputo operator. Discrete Contin Dyn Syst-S. 16(8):2118–2140. doi: 10.3934/dcdss.2023010.

Jleli M, Kirane M, Samet B. 2023. Liouville-type results for elliptic equations with advection and potential terms on the Heisenberg group. Discrete Contin Dyn Syst-S. 16(8):2141–2156. doi: 10.3934/dcdss.2022171.

Kalachev L, Graham J, Landguth EL. 2024. A simple modification to the classical SIR model to estimate the proportion of under-reported infections using case studies in flu and COVID-19. Infect Disease Modell. 9(4):1147–1162. doi: 10.1016/j.idm.2024.06.002.

Kermack W, Anderson G. 1932. Contributions to the mathematical theory of epidemics-ii, the problem of endemicity. Proc R Soc Lond, Ser-A. 138(834):55–83.
Khalid M, Sultana M, Khan FS. 2015. Numerical solution of SIR model of dengue fever. Int J Comput Appl (0975 8887). 118(21):1–4. doi: 10.5120/20866-3367.
Kongnuy R, Naowanich E, Pongsumpun P. 2011. Analysis of a dengue disease transmission model with clinical diagnosis in Thailand. Int J Math Model Methods Appl Sci. 5:594–601.
Kongnuy R, Pongsumpun P. 2011. Mathematical modeling for dengue transmission with the effect of season. Int J Math, Comput, Phys, Electr Comput Eng. 5(3):2011.
Kongnuy R, Pongsumpun P, Tang M. 2011. Mathematical model for dengue disease with maternal antibodies. Int J Med, Health, Biomed, Bioeng Pharm Eng. 5(4):2011.
Kumar M, Abbas S. 2022. Age-structured SIR model for the spread of infectious diseases through indirect contacts. Mediterranean J Math. 19(1):14. doi: 10.1007/s00009-021-01925-z.
Laarabi H, Abta A, Hattaf K. 2014 Dec 13. Optimal control of a delayed SIRS epidemic model with vaccination and treatment. Acta Biotheor. 63(2):87–97. doi: 10.1007/s10441-015-9244-1.
Ma Y, Zuo X, Owolabi KM. 2024. Stability analysis of SIRS model considering pulse vaccination and elimination disturbance. J Math. 2024(1):1–9. doi: 10.1155/2024/6617911.
Medlock J, Luz PM, Struchiner CJ, Galvani AP. 2009. The impact of transgenic mosquitoes on dengue virulence to humans and mosquitoes. Am Nat. 174(4):565–577. doi: 10.1086/605403.
Nagao Y, Koelle K. 2008. Decreases in dengue transmission may act to increase the incidence of dengue hemorrhagic fever. Proc Natl Acad Sci USA. 105(6):2238–2243. doi: 10.1073/pnas.0709029105.
Natal D. 2002. Bioecologia do Aedes Aegypti. BiolÃ‚´ogico, SËao Paulo. 64(2):205â207.
Naz R, Naeem I, Mahomed FM. 2015. A partial Lagrangian approach to mathematical models of epidemiology. Hindawi Publishing Corporation Math Probl Eng. 2015, 1–11. Article ID 602915. doi: 10.1155/2015/602915.
Olu OT, Michael OO, Emmanuel FS, Israel OO, Olufemi OS, Otonritse OJ, Olufemi OS. 2024. Numerical implementation of a susceptible-infected-recovered (SIR) mathematical model of covid-19 disease in Nigeria. WSEAS Trans Biol Biomed. 21:65–74. doi: 10.37394/23208.2024.21.7.
Parkin DM, Pisani P, Ferlay J. 1999. Global cancer statistics, CA cancer. J Clin. 49(1):33–64. doi: 10.3322/canjclin.49.1.33.
Rodrigues HS, Teresa M, Monteiro T, Torres DFM. 2013. Dengue in Cape Verde: vector control and vaccination. Math Popul Stud. 20(4):208–223. doi: 10.1080/08898480.2013.831711.
Rogers D, Onstad D, Kendrick R. 1988. The dynamics of vector-transmitted diseases in human communities and discussion philosophical transactions of the royal society of london. Biol Sci. 321(1207):513–539.
Romanullah GZ, Islam S. 2013 May-June. Stability analysis of general SIR epidemic model. VFAST Trans Math. 1:16–20.
Ryan KJ, Ray CG, Sherris JC. 2004. Sherris medical microbiology: an introduction to infectious diseases. Berlin, Germany: McGraw-Hill Medical.
Sabir Z, Raja MAZ, Javeed S, Guerrero-Sanchez Y. 2022. Numerical investigations of a fractional nonlinear dengue model using artificial neural networks. Fractals. 30(10):2240241. doi: 10.1142/S0218348X22402411.
Schieweck F. 2010. A-stable discontinuous Galerkin–Petrov time discretization of higher order. J Numer Math. 18(1):25–57. doi: 10.1515/jnum.2010.002.
Tomashek KM. 2011. Dengue fever (DF) and dengue hemorrhagic fever (DHF). CDC Health Inf For Int Travel. 11(8):532–543.
Wan H, Cui J. 2009. Model for the transmission of dengue. Researchgate. doi: 10.1109/ICBBE.2009.5162187.

Wang B, Hu Y, Cen Z, Huang J, He T, Xu A, Ben Makhlouf A. 2024. A SIR model with incomplete data for the analysis of influenza a spread in Ningbo. Discrete Dyn Nat And Soc. 2024 (1):7694770. doi: 10.1155/2024/7694770.

Wearing HJ, Rohani P. 2006. Ecological and immunological determinants of dengue epidemics. Proc Natl Acad Sci USA. 103(31):11802–11807. doi: 10.1073/pnas.0602960103.

WHO. 2003. Shaping the future, the world health report. Geneva: WHO.

Yusuf T, Benyah F. 2012. Optimal control of vaccination and treatment for an SIR epidemiological model. World J Modell Simul. 8(3):194–204.

Zaman G, Kang YH, Jung H. 2008. Stability analysis and optimal vaccination of an SIR epidemic model. Bio System. 93(3):240–249. doi: 10.1016/j.biosystems.2008.05.004.